Applied Water Science (2025) 15:221
https://doi.org/10.1007/s13201-025-02582-3

ORIGINAL ARTICLE

Projection of hydrological drought based on SSP scenarios using surface water supply index and SWAT model in mountainous watershed

Omid Babamiri[1] · Yagob Dinpashoh[1] · Alireza Samavati[2] · Faeze Shoja[3]

Received: 18 October 2023 / Accepted: 9 July 2025

Abstract

The objective of this research is to explore climate change impact on hydrological drought in mountain watersheds. The Coupled Model Intercomparison Project Phase 6 (CMIP6) models and the Soil and Water Assessment Tool (SWAT) runoff simulation model were utilized to attain the objective of the study. Moreover, the surface water supply index (SWSI) was employed to examine hydrological drought. To correct the bias of the selected CMIP6 models (ACCESS-CM2, CNRM-CM6-1, CNRM-ESM2-1, INM-CM4-8, INM-CM5-0, MIROC6, and MIROC-ES2L), the historical period from 1990 to 2014 was used as a baseline. It was found that the MIROC-ES2L model exhibited greater accuracy compared to the other chosen models in the context of the examined mountain basin, namely the Ekbatan watershed in Iran. The calibration and validation of the SWAT model were conducted using the Sequential Uncertainty Fitting version 2 (SUFI-2) algorithm, covering the calibration period from 2004 to 2017 and the validation period from 2018 to 2020. The results indicated that the model effectively simulates runoff in the watershed. The highest percentage error, as measured by the Normalized Root Mean Square Error (NRMSE), was 18.78% during the validation phase. Results from a trend analysis of runoff using the Mann–Kendall test for the projected period (2023–2042) indicate that runoff is not expected to exhibit a significant decreasing or increasing trend during this timeframe. Furthermore, an assessment of runoff uncertainty within the projected period (2023–2042) revealed that the most substantial variability or uncertainty is associated with the month of April, with a range of 0 to 9.55 m^3/s. The comparison of future runoff (2023–2042) with past runoff (2000–2020) indicates an increase in runoff during typically dry months (August, September, and October). This increase is particularly pronounced in September, where, under the SSP2-4.5 scenario and the best-performing model (MIROC-ES2L), runoff is projected to be nearly twelve times higher. This phenomenon may be attributed to the potential occurrence of intense rainfall events influenced by climate change during the dry season. Additionally, due to the generally low streamflow in this period, the relative increase appears more significant. When comparing drought conditions between the periods of 2023–2042 and 2000–2020, as assessed by SWSI, the results show that, on a 12-month scale, drought conditions in the typically wet months (February, March, April, and May) are expected to intensify under all scenarios (SSP1-2.6, SSP2-4.5, and SSP5-8.5). In other words, these months are projected to become drier in the future. The most significant increase in drought severity is anticipated in February under the SSP5-8.5 scenario, reaching a magnitude of 86.84%. Overall, results indicated an intensification of hydrological drought during the wet months in the mountainous basin.

Keywords Climate change · CMIP6 · Mann–Kendall test · Mountain watershed · SWSI · Uncertainty

✉ Omid Babamiri
babamiri@tabrizu.ac.ir

1 Department of Water Engineering, University of Tabriz, Tabriz, Iran

2 Department of Civil Engineering, Bu-Ali Sina University, Hamedan, Iran

3 Department of Physical Geography, University of Tehran, Teheran, Iran

Introduction

Drought is a complex natural event that typically starts with a lack of precipitation, resulting in reduced soil moisture and river flow, which can led to a detrimental impact on ecosystem, plant growth and human life (Li et al. 2013). Droughts that occur repeatedly are one of the various kinds of natural disasters that have a noteworthy and harmful impact on the economy, environment, and society (Mishra and Singh 2010). Droughts can be classified into the four distinct categories, namely meteorological, agricultural, hydrological, and socioeconomic. These categories are based on the types of water shortages in precipitation, soil moisture content, streamflow, and water resources (Jehanzaib et al. 2020). Among them, hydrological drought is considered the most significant as it is caused by insufficient surface or subsurface water resources (Van Loon 2015). This type of drought has a substantial impact on various sectors such as agriculture, urban life, industry, and hydropower generation, which mostly rely on surface water resources (Vasiliades et al. 2011). While most drought indices have been created for meteorological and agricultural droughts, there are also drought indices available for hydrological droughts. The Streamflow Drought Index (SDI), Palmer Hydrological Drought Index (PHDI), and Surface Water Supply Index (SWSI) are three examples of such indices (Tareke and Awoke 2022). The SDI index is similar to the Standardized Precipitation Index (SPI) in that it measures hydrological drought, but it uses streamflow data instead of precipitation. This index is suitable for studying drought at a specific site. On the other hand, the SWSI index is appropriate for hydrological drought analysis at the basin level. It takes into account various available sources of surface water, such as precipitation, streamflow, evaporation, and reservoir volume (Shafer and Dezman 1982). Therefore, given its consideration of multiple hydrological parameters, this index is expected to provide a more accurate assessment of drought conditions compared to other indices. Consequently, it is selected for this study.

It is predicted that the hydrological cycle will intensify under the influence of climate change. Moreover, future drought conditions will be altered in many parts of the world, especially in mountainous basins, due to changes in precipitation patterns, precipitation type, changes in snow accumulation, melting cycles, and increased evapotranspiration (Satoh et al. 2022). As a result, societies are likely to face a significant challenge in the future mainly due to water scarcity (Shaigan et al. 2011). Hence, to effectively plan and manage surface water resources, it is crucial to predict changes in runoff under climate change conditions, accurately (Chen et al. 2019; Liu et al. 2021). Several studies have been conducted to investigate the impact of climate change on runoff at different watersheds. Notable examples include the works of Xue et al. (2021), Kiprotich et al. (2021), Su et al. (2021), dos Santos et al. (2021), Chang and Su (2021), Lian et al. (2021), Li et al. (2021), Escanilla-Minchel et al. (2020), and Ridwansyah et al. (2020). However, none of these studies have examined the impact of climate change on runoff in mountainous basins.

Simulating runoff through hydrological models is essential for understanding the impacts of climate change on water resources and other hydrological processes studies. Accurate models are necessary for the sustainable use of water resources (Abbaspour et al. 2015). The Semi-Distributional Soil & Water Assessment Tool (SWAT) is an integrated, basin-scale model that can be used to study the hydrological and biogeochemical impacts of climate change. It is a comprehensive and accurate tool that can analyze data on different time scales such as annual, monthly, daily, and hourly basis. Developed by Dr. Jeff Arnold (1994) for the United States Agricultural Research Service, this model was designed to predict the effects of management practices on water and sediment in large and complex basins with different land uses. Its effectiveness has been demonstrated in various studies, including those by Arnold et al. (1998), Shaigan et al. (2011), and Neitsch et al. (2011). Up to now, various studies have utilized SWAT to simulate runoffs in basins, including Kamali et al. (2017), Goyal et al. (2018), Kaffas et al. (2018), Ahmadi et al. (2019), Chen et al. (2019), de Andrade et al. (2019), Babaeian et al. (2021), and Samavati et al. (2023). Due to its proven accuracy and extensive application in rainfall-runoff modeling using the SWAT model, this model has been selected for simulating runoff in this study.

To predict the future runoff of basins, it is necessary to make predictions about precipitation and air temperature. One way to project these parameters is by utilizing the IPCC reports. These parameters are then inputted into a simulation model to obtain a projection for future runoff (Khazaei and Mirzaei 2013). Some of the studies conducted to date on the impact of climate change on basin runoffs, based on projections from the Intergovernmental Panel on Climate Change (IPCC) reports and simulations of the SWAT model. Are as follows. Liu et al. (2021), used the SWAT to examine the influence of climate change on surface water in California's South-Central Valley from 2020 to 2099. The study employed four climate models (HadGEM-ESCMIP5, CNRM-CM5, CanESM2, Miroc5) and two emission scenarios (RCP4.5, RCP8.5). The results indicated that under warm weather conditions, the peak river flow was expected to increase by 0.5–4 times in the coming decades, and it would occur 2–4 months earlier in the year due to snow melting. The study also concluded that snow cover would gradually decrease in the near future, with lower rates at lower altitudes and higher rates at higher altitudes by the end of the twenty-first century. The Kelantan River catchment area in Malaysia was studied by Tan et al. (2017) using CMIP5 and SWAT models. The study involved 36 micro-scaled weather forecasts from 5 general circulation models (GCMs) across 3 Representative Concentration Pathways (RCP) scenarios (2.6, 4.5, 8.5) in the calibrated SWAT model for the time periods of 2015–2044 and 2045–2074. The findings indicated an increase in monthly rainfall during wet seasons and a decrease during dry seasons. The study concluded that monthly surface flows were likely to rise in November, December, and January, while experiencing a slight decline between June and October within the period of 2015–2044. Wodaje et al. (2021) conducted a study where they employed a collection of CMIP5 GCMs to evaluate the influence of climate change uncertainty on the flood flow of the Bilate River in Ethiopia. They utilized SWAT to simulate water flow and presented statistical evidence that the model accurately predicted the flow. The findings of the study indicated a significant increase in annual discharge for all time periods throughout the century. Specifically, under the RCP8.5 scenario, the flow during the 2080 period exhibited an approximate 42.42% increase compared to the RCP4.5 scenario. In a study conducted in 2021, Andrade et al. (2021) examined the future runoff of the Mundau River basin in Brazil. They utilized two RCMs models, namely Eta-Miroc5 and Eta-HadGEM2, and considered two scenarios, RCP4.5 and RCP8.5. They employed SWAT model to simulate the runoff of the targeted basin. The findings of their study, covering the period from 2016 to 2099, indicated a significant reduction in rainfall. Specifically, the RCP4.5 scenario showed a rainfall reduction of 0.04%, while the RCP8.5 scenario exhibited a reduction of 25.3%. A review of the literature reveals a gap in research regarding the future runoff of mountainous basins under CMIP6 climate projections.

As climate change impacts runoff, it is expected that the hydrological drought index will undergo changes in the future. To date, there have been few studies exploring the impact of climate change on hydrological drought, including: Kamali et al. (2017) investigated the effect of climate change on drought in the Karkhe River basin, Iran. They proposed the Drought Hazard Index (DHI), a combination of meteorological, hydrological, and agricultural droughts, to assess the occurrence of drought. Their findings indicated that the DHI index was an effective tool for measuring drought in future. Abdulai and Chung (2019), investigated the impact of climate change on meteorological and hydrological droughts in the Cheongmicheon basin in South Korea. The study focused on the RCP4.5 scenario of CMIP5. The results indicated the occurrence of severe or extreme short-term droughts based on the SPEI and SDI. In a study conducted by Salimi et al. (2021), the impact of climate change on hydrological and meteorological droughts was investigated. The researchers utilized the SPI, Standardized Precipitation Evapotranspiration Index (SPEI), and Standardized Streamflow Index (SSI) to analyze data from the Navrood and Lighvan watersheds in northern Iran. Their findings revealed a strong correlation between hydrological and meteorological droughts, suggesting that climate change is likely to be a major factor in the occurrence of future droughts. Lotfirad et al. (2021) examined the impact of climate change on SDI in the Central Basin of Iran. They used data from 23 General Circulation Models (GCMs) from CMIP5 and considered two scenarios, RCP4.5 and RCP8.5. The researchers used the IHACRES model to simulate the runoff of the basin. The study revealed that the basin is likely to experience short- and medium-term droughts between 2025 and 2048. Samavati et al. (2023) conducted a study to investigate the influence of climate change on the SDI in the Alvand Basin of Iran. The researchers utilized data from four (GFDL-CM3, EC-EARTH, HADGEM2-ES, and MIROC5) GCMs from CMIP5 and took into account two scenarios, RCP4.5 and RCP8.5. To simulate the runoff of the basin, the researchers employed the SWAT model. The results of the study indicated that the basin is expected to undergo an intense drought period from 2020 to 2040. Hobart et al. (2024) examined the impact of climate change on the Standardized Precipitation Index (SPI) in the Mango orchard region of Tamale, Ghana, from 2023 to 2050 using CMIP6 models and Shared Socioeconomic Pathways (SSPs). Their findings indicated that, based on SSP126 and SSP245 scenarios, the study area is projected to experience significant drought during the specified period.

A review of the literature reveals that researches on the impact of climate change on hydrological drought has primarily relied on drought indices such as SPI, SPEI, and SDI. These indices are calculated based on a single hydrological parameter, like precipitation, runoff, or evapotranspiration. However, drought is a complex phenomenon that is often associated with multiple hydrological parameters simultaneously, making it inappropriate to draw conclusions about a region's dryness or wetness solely based on a single parameter. For example, the SDI is a straightforward method that relies on a single input variable—streamflow—making it well-suited for site-specific drought assessments (Tareke & Awoke 2022). In contrast, the Surface Water Supply Index (SWSI) was developed by Shafer and Dezman (1982) at Colorado University for hydrological drought analysis at regional or basin scales. Unlike SDI, SWSI incorporates multiple surface water sources, including streamflow, precipitation, reservoir levels, and evaporation, to provide a more comprehensive evaluation of water availability (Hyung-Joong 2006). Moreover, there is limited research investigating the impact of climate change on hydrological drought in mountainous basins, which are particularly vulnerable to climate change and serve as the sources of surface water resources. To address this gap, this study aims to investigate the effects of climate change, based on CMIP6 models and scenarios, on hydrological drought in a mountainous basin. The Surface Water Supply Index (SWSI) is employed to calculate the drought index, as it incorporates precipitation, runoff, surface water evaporation, and reservoir storage volume, providing a more comprehensive assessment of drought conditions in a basin.

This study is mainly aimed to: 1. Simulating rainfall-runoff in the basin using the SWAT model and calibrating it, 2. Comparing observed and historical precipitation and temperature from GCMs during the baseline period (1990–2014), and then utilizing climate projections from 7 Model Intercomparison Project, Phase 6 (CMIP6) and SSP1-2.6, SSP2-4.5, and SSP5-8.5 scenarios for the future timeframe (2023–2043), 3. Simulating future runoff (2023–2042) in the basin based on predicted data from CMIP6 models and calibrated SWAT model parameters, 4. Evaluation of uncertainty in monthly runoff during the 2023–2042 period 5. Investigating the trend of future runoff from 2023 to 2042 using the Mann–Kendall method, 6. Estimating evaporation in the basin based on projected temperature using the best CMIP6 model for the basin, 7. Estimating the volume of the dam reservoir using hydrological data projected by the best CMIP6 model, and 8. Calculating the SWSI for the best model from 2023 to 2042 and comparing it with past data (2000–2020).

Materials and methods

The study area

The sub-basin of the Central Zagros Basin in western Iran, known as the mountain watershed of Ekbatan Dam, spans from longitude 3,831,000 to 38,493,000 and latitude 268,000 to 287,000. The catchment area of Ekbatan Dam, which has an elevation range of 1970 to 3467 m, covers an area of 221.55 km^2. Figure 1 shows the location of Ekbatan dam watershed in Iran. The Eberoo and Yalfan rivers both converge at the Ekbatan dam, which supplies the water

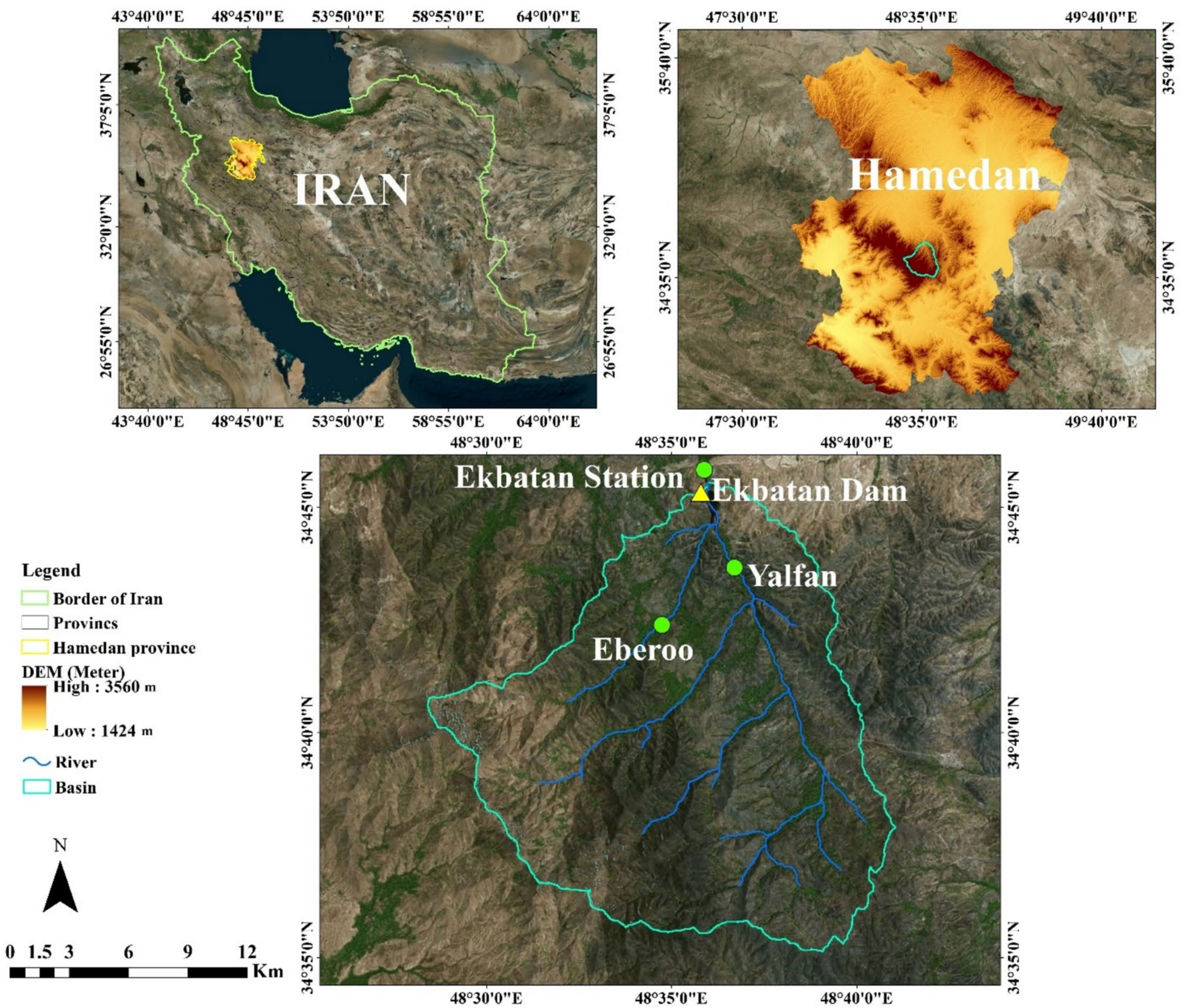

Fig. 1 The site Location of Ekbatan mountain watershed, Iran

demands of Hamedan city from this reservoir. Based on the data from Hamedan synoptic station, the average precipitation, average maximum temperature, and average minimum temperature in the basin are 316.73 mm, 20.2 °C, and 4.4 °C, respectively (http://www.irimo.ir). The Köppen Geiger (Kottek et al. 2006) climate classification characterizes the basin's climate as semi-arid.

SWAT model

This study uses a semi-distribution physical hydrological model known as SWAT to simulate and predict long-term runoffs, sedimentations, and chemical-agricultural products in a watershed. The simulation of hydrological processes is done in two phases: ground or soil profile and routing (Arnold et al. 1998). The ground phase calculates the inflow of water, sediments, nutrients, and pesticides to the main channel in each reservoir based on the water balance concept that considers processes such as rainfall, evapotranspiration, seepage, surface runoff, lateral flow, and groundwater flow. The routing phase uses the main channel to connect all sub-basins and simulates the movement of water and sediment towards the basin outlet (Cibin et al. 2010; Chen et al. 2019). Interflow in SWAT is calculated using a linear function that takes into account factors like slope length and angle, saturated conductivity, soil porosity, and the amount of water stored in the saturated zone (Gebremariam et al. 2014). SWAT simulates hydrological cycles based on the water balance equation (Eq. 1).

$$SW_t = SW_0 + \sum_{i=1}^{t} \left(R_{day} - Q_{surf} - E_a - W_{seep} - Q_{gw}\right) \quad (1)$$

where SW_0 and SW_t (mm) represent the initial and final soil water levels, and R_{day}, Q_{surf}, E_a, W_{seep}, and Q_{gw} (mm) correspond to the rainfall, runoff, evapotranspiration, interflow, and base flow, respectively on the ith day, respectively.

SWAT input data

The Spatial Analyst feature within ArcGIS software is employed by SWAT to create flow networks and basin boundaries, utilizing the digital elevation model (DEM) and raster primary functions, as detailed by Abbaspour et al. in 2007. Initially, the DEM10 map was acquired from the Natural Resources Department in Hamedan Province for modeling purposes, as shown in Fig. 2a. Since the waterway and sub-basin network was not previously delineated, it

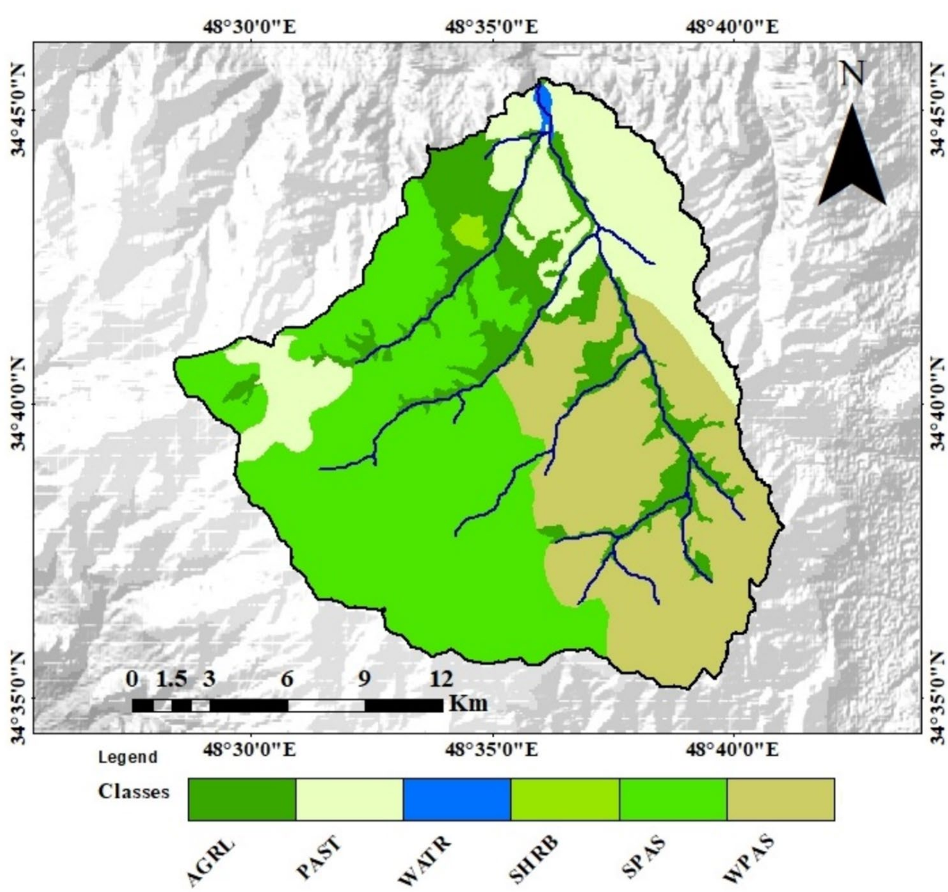

Fig. 2 Land use map of the study area

was established using the "flow direction and accumulation" technique and subsequently examined in Google Earth, as illustrated in Fig. 2b. This network and its associated basins were further subdivided into 27 sub-basins, as displayed in Fig. 2c. Due to the absence of a provincial soil map, a global soil map was employed, and the land use map, depicted in Fig. 2d, was obtained from the aforementioned unit and integrated into the GIS model.

Table 1 provides an overview of the characteristics of synoptic and hydrometric stations within the Ekbatan basin. Specifically, Eberoo and Yalfan hydrometric stations are responsible for gauging runoff within the basin, while the Ekbatan Dam station, positioned at the dam's outlet, records and monitors rainfall data. Furthermore, meteorological parameters such as air temperature, radiation, wind speed, and relative humidity are meticulously measured and documented at the Hamedan station, located in close proximity to the watershed. These meteorological data points play a crucial role in simulating watershed runoff through the implementation of the SWAT model. It is imperative to maintain data consistency and completeness when inputting information into the SWAT model to prevent potential errors or discrepancies within the model.

Future climate scenarios (CMIP6 SSP Scenarios)

A new generation of GCMs developed for CMIP6 have been published by the IPCC (AR6) which is now available. These experiments are based on advanced GCMs that more accurately represent the complex physical processes within the climate system than previous GCMs (Wang et al. 2018; Siabi et al. 2023). Based on the most recent trends in anthropogenic carbon emissions, CMIP6 introduced a new projection scenario known as the rectangular combination of SSPs and RCPs (Peng & Li 2021). In general, new SSPs are scenarios that, in addition to previous RCP concepts, take into account future socio-economic changes and contribute to mitigate climate change. Nevertheless, the CMIP6 climate projections differ from the previous phase (CMIP5), not only because of newer forms of climate models coupled with SSP scenarios, but also because they show new gap scenarios that were not previously covered (Siabi et al. 2023). CMIP6 contains seven scenarios: The four scenarios SSP1-2.6, SSP2-4.5, SSP4-6.0, and SSP5-8.5 are the updated RCP2.6, RCP4.5, RCP6.0, and RCP8.5 scenarios available in CMIP5, and the scenarios SSP1-1.9, SSP4-3.4, SSP3-7.0 are newly added to this project (Gupta et al. 2020). Although the historical simulations of CMIP6 cover the period 1850–2014, the current study considered the 20-year period 1990–2014 to be the baseline period and corresponded to the station period. To analyze the GHG emission scenarios in each model under different climate policies, minimum temperature, maximum temperature and precipitation from the output of 7 GCMs based on SSP1-2.6, SSP2-4.5, SSP5-8.5 for the near future period (2023–2042) were obtained from the ECMWF-COPERNICUS website at https://cds.climate.copernicus.eu/. The specifications of the GCMs used in the study and their development institutions are listed in Table 2.

Table 1 Specifications of the stations used in the study area

Station type	Station name	Latitude	Longitude	Elevation (m)	Data collection period
Hydrometric	Ekbatan	34°,45′,28″	48°,35′,59″	1935	2000–2020
Hydrometric	Yalfan	34°,43′,43″	48°,36′,38″	2074	2000–2020
Hydrometric	Eberoo	34°,42′,48″	48°,35′,6″	2196	2000–2020
Synoptic	Hamedan	34°,46′,46″	48°,33′,5″	1922	2000–2020

Table 2 Characteristics of the 8 CMIP6 GCMs used in this study (Babaousmail et al. 2022)

No	Model name	Modeling center (or Group)/Country	Atmospheric resolution (lon × lat)
1	ACCESS-CM2	Commonwealth Scientific and Industrial Research Organisation/Australia	1.25° × 1.875°
2	CNRM-CM6-1	Centre National de Recherches Météorologiques–Centre Européen de Recherche et de Formation Avancée en Calcul Scientifique/France	1.4° × 1.4°
3	CNRM-ESM2-1		
4	INM-CM4-8	Institute for Numerical Mathematics/Russian Academy of Science/Russia	1.5° × 2°
5	INM-CM5-0		
6	MIROC6	Japan Agency for Marine-Earth Science and Technology, Atmosphere and Ocean Research Institute, The University of Tokyo, National Institute for Environmental Studies, and RIKEN Center for computational Science/Japan	1.4° × 1.4°
7	MIROC-ES2L		

Bias correction method

A variety of methods have been developed to bias the output of GCMs, ranging from simple scaling methods to more complex distribution mapping methods (Luo et al. 2018). Linear scaling (LS) is an effective technique in this case (Yao et al. 2021). The monthly average of the corrected values is fully consistent with the observed values in the LS method. This method typically corrects precipitation with a multiplier and temperature with an additive value on a monthly basis, as demonstrated in Eqs. (2) and (3), respectively. The assumption is that there will be no change in the correction factors and additives in use, even under future conditions (Teutschbein & Seibert 2012; Luo et al. 2018).

$$P^{cor}_{hst,m,d} = P_{hst,m,d} \times \left[\frac{\mu\left(P_{obs,m}\right)}{\mu\left(P_{hst,m}\right)}\right] \tag{2}$$

$$T^{cor}_{hst,m,d} = T_{hst,m,d} + \left[\mu\left(T_{obs,m}\right) - \mu\left(T_{hst,m}\right)\right] \tag{3}$$

$P^{cor}_{hst,m,d}$ and $T^{cor}_{hst,m,d}$ are the corrected precipitation and temperature on the dth day of the mth month, respectively; $P_{hst,m,d}$ and $T_{hst,m,d}$ represent the precipitation and temperature resulting from the main outputs of the GCM in the respective period. The subscripts d and m denote specific days and months, respectively, and μ indicates the average value.

Surface water supply index (SWSI)

Shafer and Dezman (1982) developed the SWSI in Colorado as a supplement to the Palmer Drought Severity Index. SWSI considers streamflow, reservoir storage, and snowpack when assessing drought severity. To calculate the SWSI for a particular basin, the following steps are taken: monthly data from reservoir inflow, streamflow monitoring stations, and precipitation stations within the basin are collected and combined. The sum of each component is then standardized using a long-term average. Additionally, weights are assigned to each element based on its frequency of contribution to the basin's surface water (Tareke and Awoke 2022). The SWSI equation is given below in Eq. (4):

$$\mathrm{SWSI} = \frac{\mathrm{aPNstrm} + \mathrm{bPNpre} + \mathrm{cPNrvol} - 50}{12} \tag{4}$$

In this equation, SWSI represents the Surface Water Supply Index. PNstrm, PNprec, and PNrvol are expressed as a percentage of non-exceedance for monthly streamflow, precipitation, and reservoir storage volume, respectively. The weights for each hydrologic component are denoted by a, b, and c, with the condition that their sum equal to 1. By subtracting 50 from the calculated values, the SWSI values are centered around zero. Additionally, dividing by 12 compresses the range of values between −4.2 and +4.2. The non-exceedance probabilities are derived from probability distributions fitted to each hydrologic component.

The Eq. (5) represents the formulation of the weighted factors a, b, and c.

$$\mathrm{P_a} = \mathrm{P_b} = \mathrm{P_c} = \frac{\mathrm{X_i}}{\mathrm{X_{Max}}} \tag{5}$$

The proportional values of monthly or annual streamflow, precipitation, and reservoir storage are represented by P_a, P_b, and P_c, respectively. The observed monthly or annual value is denoted as X_i, while the maximum values for all components are represented as X_{max}. The weighted factors can be determined using Eq. (6).

$$\mathrm{a} = \frac{\mathrm{P_a}}{\mathrm{P_t}},\ \mathrm{b} = \frac{\mathrm{P_b}}{\mathrm{P_t}},\ \mathrm{c} = \frac{\mathrm{P_c}}{\mathrm{P_t}} \tag{6}$$

where: P_a, P_b, and P_c refer to the proportionality of each component. The total proportionality of all components is represented by P_t, which is equal to the sum of P_a, P_b, and P_c. The weighted factors for each surface water component (streamflow, precipitation, and reservoir storage) are represented by a, b, and c, respectively.

Using Eq. (7), the probability of non-exceedance was calculated for each component.

$$PN = 1 - \frac{m}{n+1} \tag{7}$$

where PN represents the non-exceedance probability of each component, while m denotes the rank, and n signifies the total number of data points taken into account in the time series.

Based on the remarks of Shafer and Dezman, Table 3 classifies SWSI values into eight categories.

The monthly reservoir storage of Ekbatan Dam from 2023 to 2042 was determined through the Standard Operating Policy (SOP) method, as outlined in Loucks et al. (1981). As well, the calculation of evaporation from both

Table 3 Drought classification based on SWSI

Class	SWSI range	Description
A	≥ +4	Abundant supply
B	3.99 to 1.99	Wet
C	2 to −0.99	Normal
D	−1 to −1.99	Incipient drought
E	−2 to −2.99	Moderate drought
F	−3 to −3.99	Severe drought
G	≤ −4	Extreme drought

the dam lake and its watershed was executed using the Hargreaves and Samani (1985) method.

The general flowchart of the present study is shown in Fig. 3. In this study, initially, the necessary data for runoff simulation using the SWAT model is inputted and the model is calibrated and validated for the study area. Subsequently, climate parameters are projected using CMIP6 models and scenarios and bias-corrected. The projected data is then inputted into the SWAT model to simulate future runoff. The trends and uncertainties in the simulated runoff are subsequently analyzed. In the final stage, the SWSI is calculated using the simulated runoff, precipitation, and reservoir storage volume data.

Results

Calibration and validation of SWAT model

Calibrating a hydrological model is a subjective process that requires the researcher's knowledge of their study area. No automatic algorithm can replace this expertise. As a result, it is important to closely link calibration procedures with uncertainty analysis, and to quantify the degree of uncertainty associated with the model prediction before performing any calibration (Abbaspour et al. 2015; de Andrade et al. 2019). The warm-up period for this study, which had a significant positive impact on the statistical results, spanned from 2000 to 2003. The calibration period covered the years 2004 to 2017, while the validation period included the years 2018 to 2020. Given the challenging nature of the mountainous study basin and the complexities involved in obtaining results, the input parameters were handled on the sub-basin level. Table 4 presents a list of 16 highly sensitive parameters, including their descriptions and calibrated values, which were used for monthly runoff calibration.

Results showed that, the optimal average value of the curve parameter (r__CN2) for the basin was determined to be −0.209. It is noteworthy that this calibration result for the CN parameter aligns with the findings of Hammouri et al. (2017). The Baseflow alpha-factor (ALPHA_BF) exhibited a range of variability from 0 to 1 day, and it was determined through calibration to have a value of 0.726. This finding aligns with the results reported by Fereidoon et al. (2019).

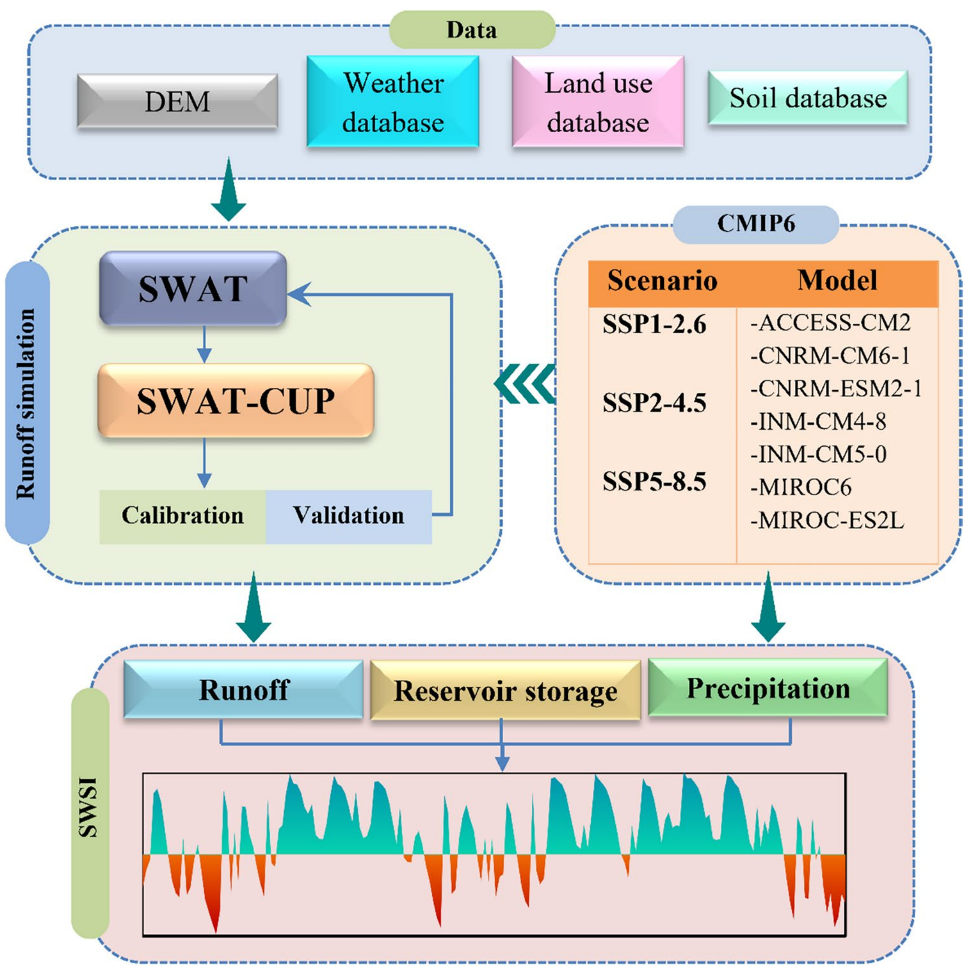

Fig. 3 The proposed modeling framework in the present study

Table 4 SWAT model parameters calibrated and adjusted values for Ekbatan watershed

No	Parameter	Description	Initial range	Calibrated value
1	r__CN2.mgt	Curve Number, moisture condition II	−0.2 ~ 0.2	−0.209
2	v__ALPHA_BF.gw	Baseflow alpha factor (days)	0.0 ~ 1.0	0.726
3	v__GW_DELAY.gw	Groundwater delay, days	30 ~ 450	314.561
4	v__GWQMN.gw	Depth of water in shallow aquifer required for return flow, mm	0 ~ 5000	4925.482
5	v__GW_REVAP.gw	Groundwater "revap" coefficient	0.02 ~ 0.2	0.154
6	v__CH_N2.rte	Manning's "n" value for the main channel	−0.01 ~ 0.3	0.263
7	v__CH_K2.rte	Effective hydraulic conductivity in main channel alluvium	−0.01 ~ 500	6.332
8	r__SOL_AWC(1).sol	Available water capacity of the soil layer	−0.2 ~ 0.4	0.272
9	r__SOL_K(1).sol	Saturated hydraulic conductivity	−0.8 ~ 0.8	0.482
10	r__SOL_BD(1).sol	Moist bulk density	−0.5 ~ 0.6	0.403
11	r__HRU_SLP.hru	Average slope steepness	0 ~ 0.2	0.0089
12	v__OV_N.hru	Manning's "n" value for overland flow	0.1 ~ 30	36.738
13	r__SLSUBBSN.hru	Average slope length	0 ~ 0.2	0.0021
14	v__SMFMX.bsn	Maximum melt rate for snow during year (occurs on summer solstice)	0 ~ 10	1.641
15	v__SMFMN.bsn	Minimum melt rate for snow during the year (occurs on winter solstice)	0 ~ 10	12.874
16	v__SURLAG.bsn	Surface runoff lag time	0.05 ~ 24	3.148

The groundwater delay time (GW_DELAY) ranges from 0 to 500 days, which is the default limit in the SWAT model. In this study basin, the calibrated value for GW_DELAY was approximately 315 days. Comparatively, de Andrade et al. (2019) recorded a value of 135 days for the Mundau´ River basin, while Xue et al. (2014) obtained a calibrated value of 101 days for the Huolin Basin in China when analyzing the surface current uncertainty parameter and sediment production. In contrast, Blainski et al. (2017) recorded a value of 0.65 for the Camboriu´ River Basin, indicating that the time interval required for underground feeding was less than one day. These variations highlight the significant influence of drainage zone size on the GW_DELAY parameter. The amount of return flow (GWQMN) from groundwater is influenced by factors such as rainfall and evapotranspiration, with capillary flow playing a significant role. The calibrated value of 4925.5 mm suggests that the water level must be at least approximately 4.9 m deep for return flow to occur in the catchment areas of the region. The mean value of the calibration for the average slope steepness (r__HRU_SLP.hru) was 0.0089. Similarly, the average slope length (r__SLSUBBSN.hru) had a value of 0.0021. The calibrated value for the Surface runoff lag time coefficient (SURLAG) in this area was 3.148, which can range from 0.5 to 24. In the Gharehsoo River basin in Iran, Taie Semiromi and Koch (2019) obtained a SURLAG value of 3.63. Bhatta et al. (2019) obtained a value of 0.56 in the Tamor River basin in Nepal. Aliyari et al. (2019) calibrated the SURLAG for the Pallet River Basin in Colorado at 6985. In this research, the Manning coefficient calibration value (v__CH_N2.rte) was determined to be 0.263. In a study conducted by de Andrade et al. (2019), the calibration value for CH_N2 was reported as 0.34. In the investigated basins, Rajib et al. (2016) identified adjusted CH_N2 values ranging from 0.02 to 0.15. Zhang et al. (2015) determined this parameter to be 0.03 in the Jinjiang River Basin in China. Pereira et al. (2014) obtained a CH_N2 value of 0.011 for the Headwater basin in southern Brazil. Additionally, the calibrated value for the effective hydraulic conductivity of CH_K2 in the main channel alluvium in our study was found to be 67.57. The calibrated value for the Available soil moisture capacity (r__SOL_AWC(1).sol) can range from −60 to + 60%. Different soil types have values ranging from −0.2 to 0.4 mm/mm. In this watershed, the calibrated value was 0.272. Aliyari et al. (2019) obtained the calibrated value of SOL_AWC for the Pallet River Basin in Colorado at 0.9136. The calibrated value for saturated hydraulic conductivity (r__SOL_K(1).sol) was determined to be 0.482. As noted by Andrade et al. (2013), saturated hydraulic conductivity typically exhibits significant spatial variability. The SWAT model, however, does not consider this spatial distribution but instead relies on an average value for a specific soil type. Consequently, the model derives the maximum permissible value during the calibration phase through the optimization process. The range for the Moist bulk density (r__SOL_BD(1).sol) is from −0.5 to 0.6%. For the watershed under study, this value was determined to be 0.403.

Evaluating model calibration involves comparing the simulated and observed hydrographs, which is an important procedure (Andrade et al. 2013; Babamiri et al. 2022). Figure 4 displays the hydrographs observed and simulated by the SWAT model for the calibration and validation phases, using monthly time steps, at the Yalfan and Eberoo streamflow gauge stations in the Ekbatab dam watershed. In this

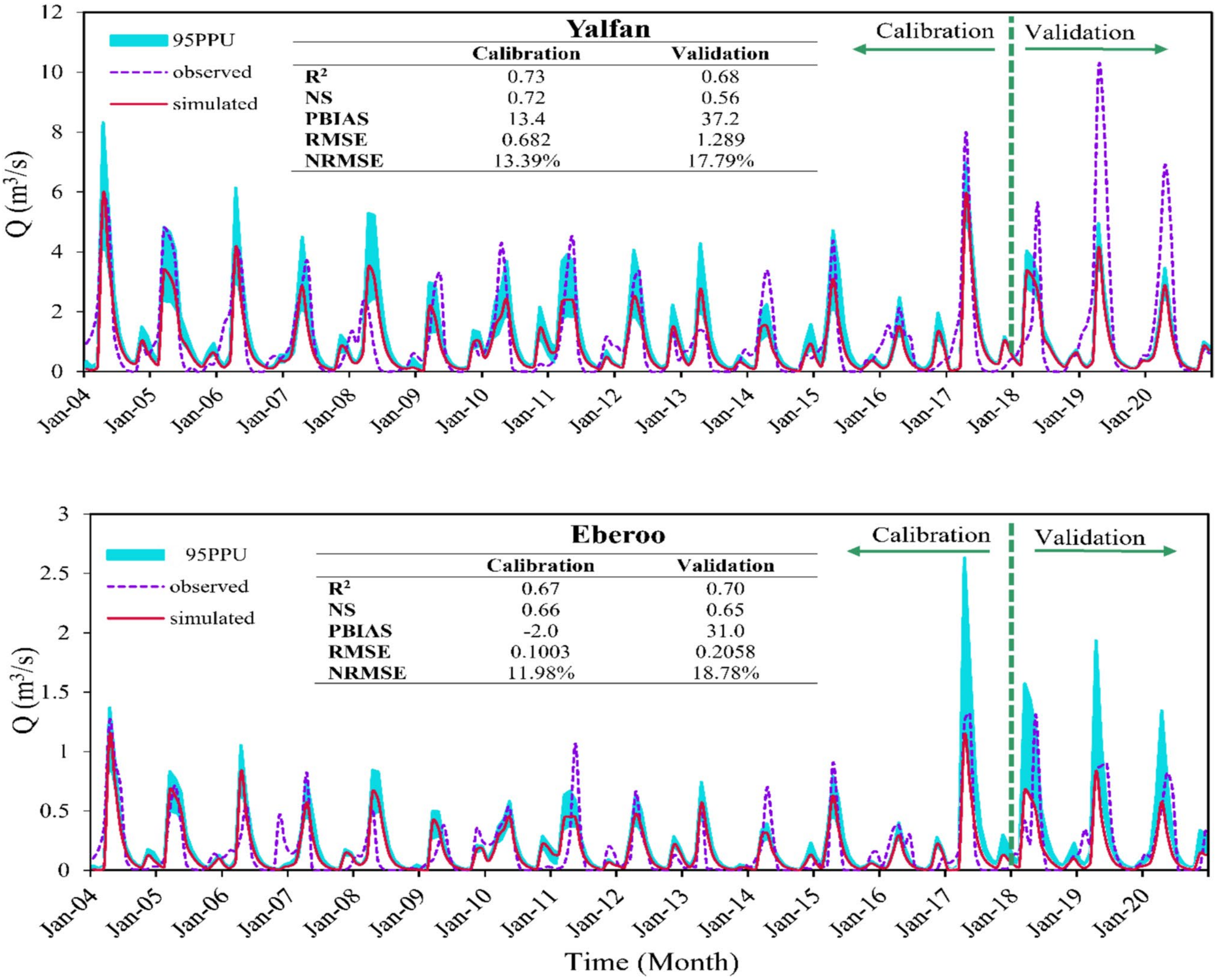

Fig. 4 Comparison of the simulated monthly runoffs with observed values in Yalfan and Eberoo hydrometric stations; *95PPU: 95 Percent Prediction Uncertainty*

study, to warm up the model, data from 2001 to 2003 were utilized. The calibration period spanned from 2004 to 2017, accounting for 70% of the total data period, as is common in similar studies. The extended calibration period was specifically designed to enhance the model's ability to accurately simulate peak runoff events, a known challenge for SWAT model.

The comparison revealed a satisfactory fitting between the measured and simulated hydrographs. While the model performed well in simulating overall basin runoff, certain discrepancies were observed in the simulation of peak flow, particularly at the Yalfan station during the validation period. To enhance the model's accuracy, especially in capturing peak flows, the calibration period, 70% of the data, was employed. However, the Nash–Sutcliffe Efficiency (NSE) value at the Yalfan station during validation was 0.56, which, according to Moriasi et al. (2007), is considered adequate for SWAT model. Notably, the model's primary errors were confined to peak flow simulation, while the overall trend of simulated and observed runoff exhibited no significant differences. The range of R^2 for both stations in calibration and validation was in the range of 0.67 to 0.73. The NS coefficient for calibration was 0.72 and 0.66 for the Yalfan and Eberoo stations, respectively, and it was 0.56 and 0.65 for validation, respectively. The percentage of error according to the NRMSE coefficient was 13.39% and 11.98%, respectively for Yalfan and Eberoo stations in the calibration stage. In the validation stage, this value was 17.79% and 18.78%, respectively. In general, according to the above criteria, the SWAT model has a satisfactory simulation in runoff based on Moriasi et al. (2007) proposed classification.

Evaluating the selected CMIP6 models

The maximum and minimum air temperature dataset were obtained for Hamedan station, while precipitation data were collected for Ekbatan station. For the current study, the 20-year period from 1995 to 2014 was selected as the baseline period for bias correction and selecting the best model.

Figure 5 presents the Taylor diagrams for chosen models before and after bias correction. This diagram enables simultaneously the assessment of correlation, error, and the comparison of standard deviation between multiple model outputs and observed values. In this figure, the observational data is marked by a red square point (OBS), while the selected models of CMIP6 are represented by dots of different colors. Based on the Fig. 5(a), prior to implementing bias correction, the MIROC-ES2L model outperforms other models for the precipitation parameter. This superiority is attributed to its proximity to the observation point, resulting in an RMSE of 10.3 (mm/month) and an R-value of 0.88. Regarding the maximum temperature, the MIROC-ES2L and ACCESS-CM2 models appear to be the most accurate compared to other models. This is due to their proximity to the observation point and high R values of 0.99, as well as RMSE values of 1.97 and 1.98 mm/month, respectively (Fig. 5b). Furthermore, prior to bias correction, when assessing minimum temperature,

Fig. 5 Taylor diagrams to compare the selected models of CMIP6 for precipitation (upper panel) T_{max} (middle panel), and T_{min} (bottom panel)

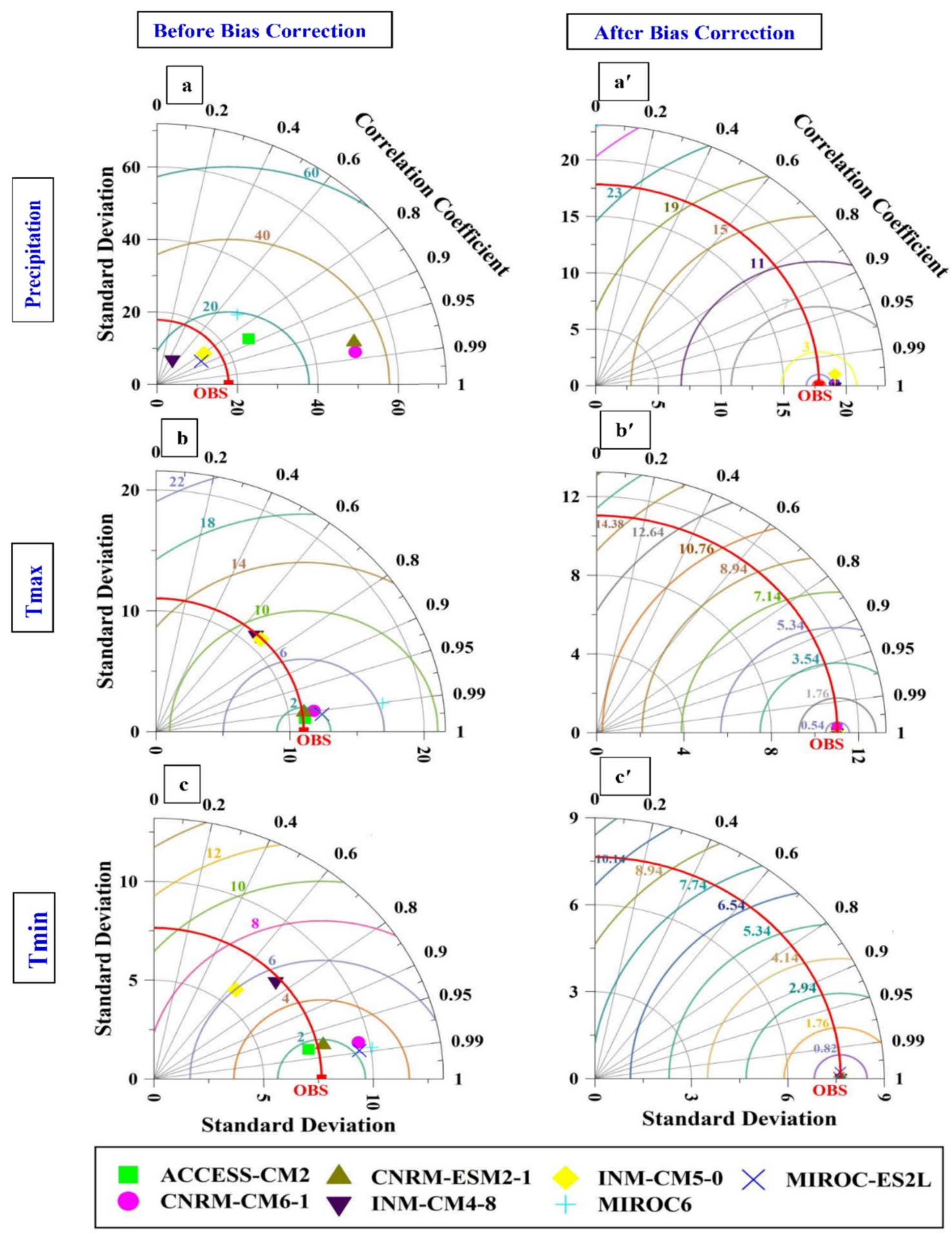

the MIROC-ES2L model exhibits the least error in comparison to alternative models, with an RMSE of 2.1(mm/month) and an R-value of 0.98 (Fig. 5c). Following the bias correction, all models show a negligible error in their parameters. In other words, all indicators match the observation data indicator precisely (a′, b′ and c′ of Fig. 5).

Evaluating of the future runoff under selected models and scenarios

Figures 6 and 7 display the projected runoff for Yalfan and Eberoo stations using the SWAT model, based on CMIP6 models (ACCESS-CM2, CNRM-CM6-1, CNRM-ESM2-1, INM-CM4-8, INM-CM5-0, MIROC6, and MIROC-ES2L) across three different scenarios (SSP1-2.6, SSP2-4.5, and SSP5-8.5). As depicted in Fig. 6, it can be inferred that the ACCESS-CM2 model predicts a higher runoff compared to the other models at the mentioned stations. Conversely, the CNRM-ESM2-1 model projects the lowest runoff within the study area.

To examine the future runoff (2023 to 2042) trend, the Mann–Kendall (MK) method [Mann (1945) and Kendall (1975)] was employed. The Z and S criteria of the MK test are presented in Table 5. It can be seen that in most of the runoff series, the future runoff does not have a significant trend under the investigated models and scenarios. Except for the runoff related to models INM-CM5-0 under the SSP1-2.6 scenario and CNRM-CM6-1 under the SSP5-8.5 scenario, which respectively have a positive and significant trend at the 10% and 5% levels. The trend line shows a positive slope in all models for the SSP1-2.6 scenario, except for the MIROC-ES2L model. In simpler terms, runoff is generally increasing, though this increase is not statistically significant.

Table 6 illustrates the percentage of runoff changes between 2023 and 2042 in comparison to the period from 2000 to 2020, on a monthly basis. It can be seen that, the month of September shows the highest increase in runoff among all months in all the studied scenarios, with averages of 863%, 1017.98%, and 820.98% for the SSP1-2.6, SSP2-4.5, and SSP5-8.5 scenarios, respectively. Conversely, the month of July exhibits the highest decrease in runoff among all the studied scenarios, with percentages of − 49.70%, − 42.54%, and − 49.77% for the SSP1-2.6, SSP2-4.5, and SSP5-8.5 scenarios, respectively.

The most significant rise in runoff is associated with the month of September in the SSP2-4.5 scenario and the CNRM-ESM2-1 model, amounting to a 1438.7% increase. Conversely, the most substantial reduction in runoff occurs during July under the SSP5-8.5 scenario and the INM-CM5-0 model, resulting in a decrease of − 71.85%.

Generally, across all scenarios, there will be a decline in runoff from January to July and an upsurge in runoff from August to December compared to previous periods.

Uncertainty analysis

To explore the spectrum of potential runoff variations in the future using the SWAT model within the scope of the studied models, we initiated the process by generating monthly average temperature and precipitation data from these models (Babamiri and Dinpashoh 2024). Subsequently, discrepancies computed for each model in comparison to the base period average (Muronda et al. 2021), visualizing these variations through a Villon diagram. Moving forward, we constructed a violin plot specifically for the runoff data derived from the CMIP6 models under investigation (Fig. 8). As indicated in the figure, a discernible pattern emerges wherein both the highest and lowest temperatures exhibit a consistent seasonal progression. The most significant variations in these stochastic parameters manifest during the colder months of the year, typically around 20 degrees Celsius. As observed (Fig. 8c), there is a substantial fluctuation in precipitation during the wet months, whereas during the dry months (June, July, August, September), precipitation is minimal or virtually absent. The most significant variations occur in March and April, with values ranging approximately from 0 to 260 mm. The majority distribution of precipitation during the March and April falls within the 0 to 75 mm range. In April, the interquartile range spans from 32.2 to 73.5 mm, while in March, it spans from 29.3 to 65.2 mm.

It is evident that despite minimal precipitation from June to September, runoff persists due to the mountainous terrain and the presence of snow reserves in the study area (Fig. 8d). The most notable variations in runoff occur during April and May, typically ranging from 0 to 9.4 cubic meters per second. The predominant distribution of runoff during these months falls within the 0 to 3.5 m^3/s range. Specifically, in April, which experiences the highest runoff levels, the interquartile range spans from 1.82 to 3.88 m^3/s.

Evaluating of the surface water supply index (SWSI)

Shafer and Dezman (1982) developed the SWSI in Colorado as a supplement to the Palmer Drought Severity Index. SWSI considers streamflow, reservoir storage, precipitation, and evaporation when assessing drought severity. Figure 9 shows the SWSI values on a monthly basis for the period of 2007 to 2022, with time scales of 1, 3, 6, and 12 months. For the time windows of 1 and 3, the SWSI value is mostly within the range of − 0.99 to 4, indicating normal, and wet conditions in the watershed. However, there were a few months having negative SWSI values in

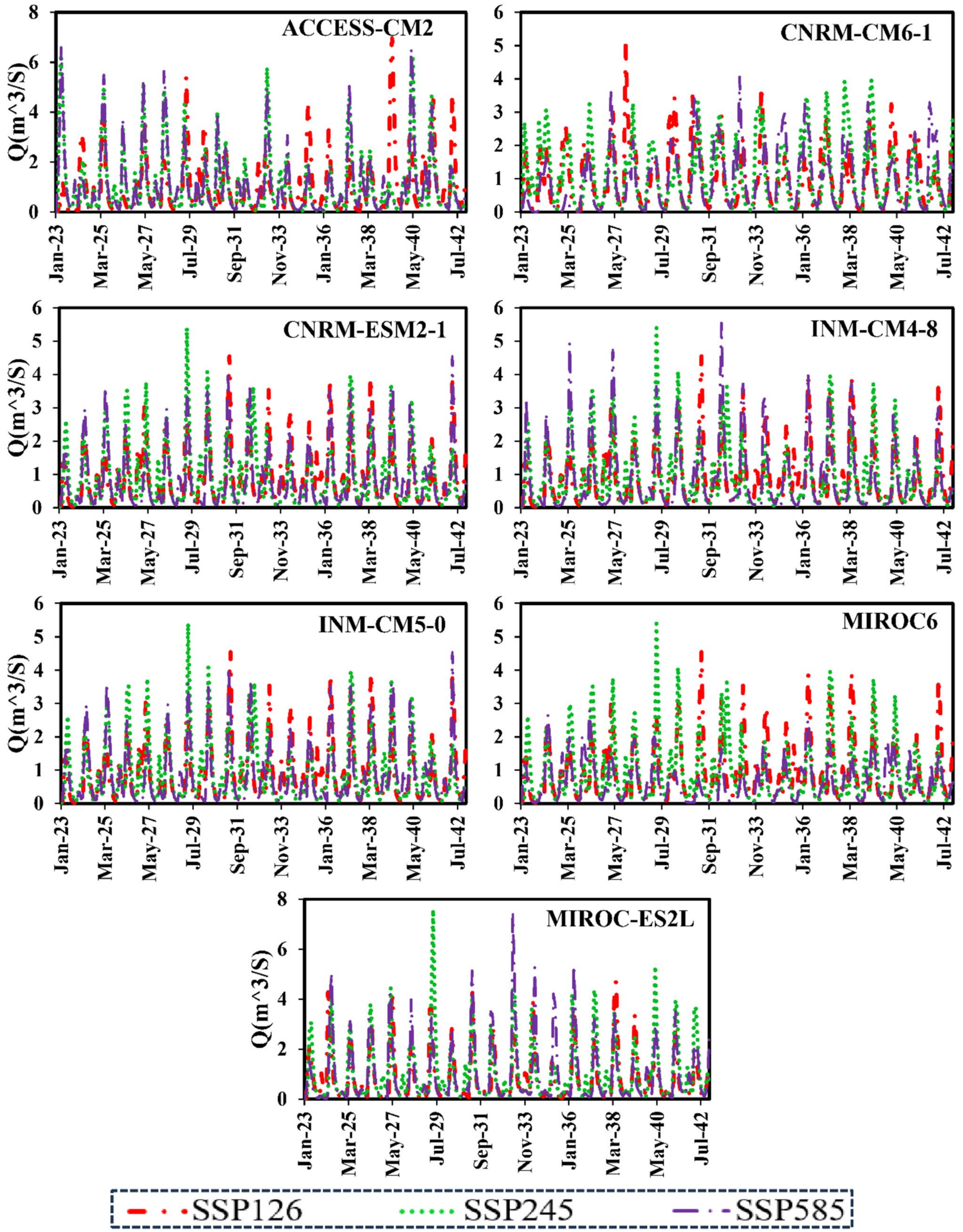

Fig. 6 Runoff simulated with CMIP6 models for Yalfan stations during 2023 to 2042

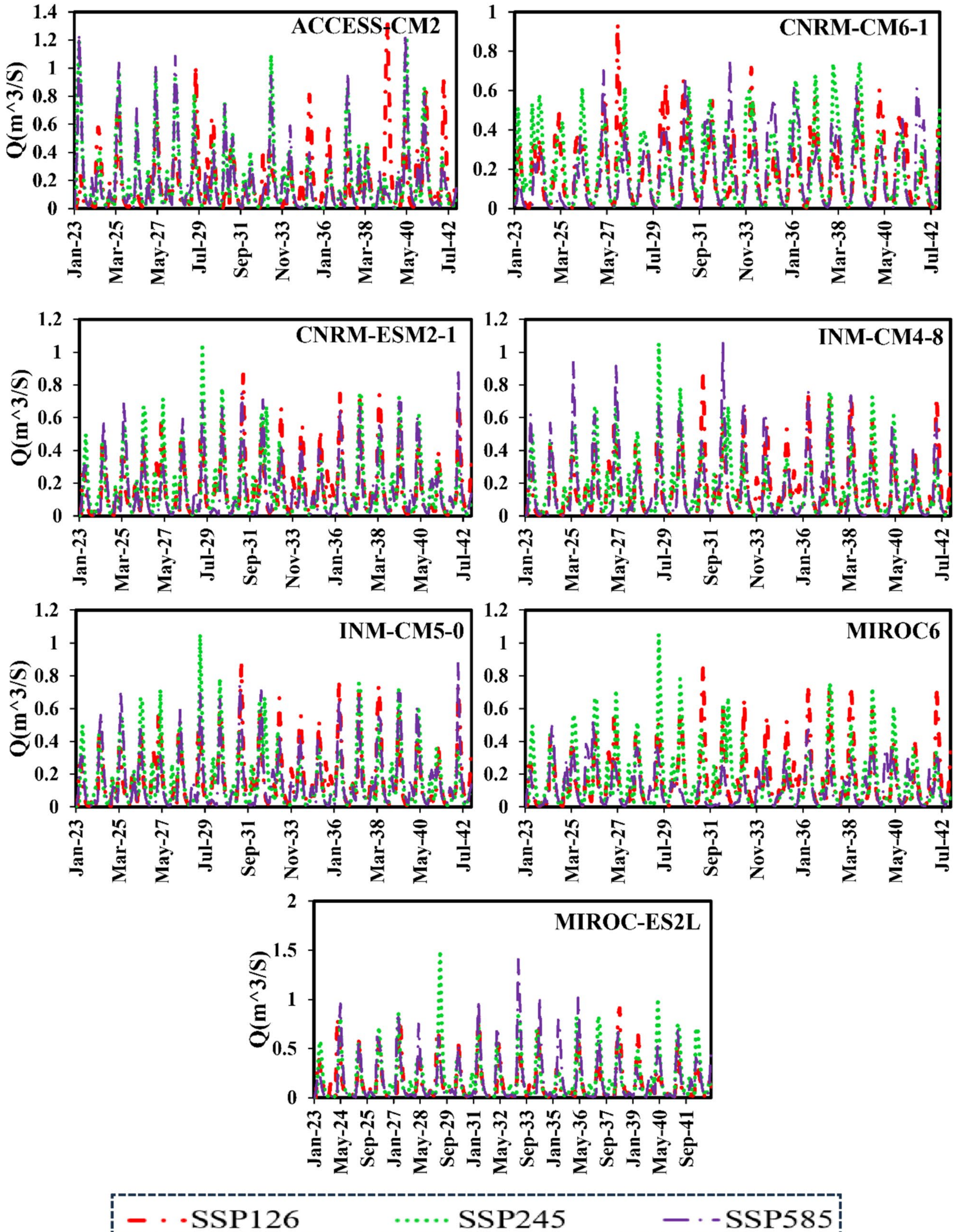

Fig. 7 Runoff simulated with CMIP6 models for Eberoo stations during 2023 to 2042

Table 5 The Z and S values obtained for runoff in monthly timescale using the Mann–Kendall test

Model	SSP1-2.6		SSP2-4.5		SSP5-8.5	
	Test Z	S	Test Z	S	Test Z	S
ACCESS-CM2	1.52	0.30	−1.33	−0.32	−1.20	−0.43
CNRM-CM6-1	0.42	0.05	−0.36	−0.10	*2.24***	0.45
CNRM-ESM2-1	1.46	0.24	−0.75	−0.15	1.52	0.18
INM-CM4-8	1.52	0.36	−0.81	−0.13	−0.16	−0.02
INM-CM5-0	*1.72**	0.23	0.42	0.09	0.16	0.02
MIROC6	0.03	0.01	0.10	0.03	0.10	0.02
MIROC-ES2L	−1.14	−0.09	1.52	0.22	0.23	0.02

The values indicated in italics with an asterisk, and with two asterisks denote to be significant at 5, and 1 percent levels, respectively

2008, 2013, and 2022 when the basin encountered moderate to severe drought conditions (Fig. 9a and b). Based on time window 6, it can be affirmed that the most severe drought occurred between April and July of 2022 (Fig. 9c).

In the context of a 12-month time scale (Fig. 9d), which serves as the main hydrological drought indicator (Mishra and Singh 2010), the basin's drought history is as follows: From July 2007 to May 2008, the basin endured a period of severe drought. Between October 2012 and May 2013, the basin experienced moderate drought. The basin experienced wet conditions from January 2018 to April 2020. However, from May 2021 to January 2022, the basin underwent another severe drought episode.

Figures 10, 11, and 12 show the projected SWSI time series from 2023 to 2042 for the best model (MIROC-ES2L) across three distinct scenarios: SSP1-2.6, SSP2-4.5, and SSP5-8.5.

Under the SSP1-2.6 scenario, Fig. 10 shows that the basin is likely to experience normal and wet conditions based on a one-month timescale from November 2029 to July 2040. On the other hand, it is expected to undergo severe drought during the dry months of 2023, 2024, 2025, and 2041. The SWSI trend in the three-month and six-month timeframes would be similar to the one-month pattern, except for an extended duration of drought during dry months. In a 12-month timescale from 2029 to 2038, the basin is projected to maintain normal and wet conditions. However, it's important to note that moderate or severe drought is expected in 2023, 2025, 2028, and during the period between February 2040 and March 2041.

Figure 11, under the SSP2-4.5 scenario, indicates that the basin will experience normal and wet conditions in terms of dryness within a one-month timescale from February 2026 to November 2033. The trend in the three-month and six-month timescales is similar to that of the one-month. However, in a 12-month timescale from January 2033 to February 2036, the basin is expected to encounter moderate to severe drought. The most severe drought conditions are anticipated to occur in February and March 2034, as well as September and October 2041.

According to Fig. 12 in the SSP5-8.5 scenario, the basin is projected to experience wet conditions under all timescales from January 2038 onwards. However, when considering the twelve-month time scale, there will be two periods of severe drought in the basin from May 2026 to April 2027 and from December 2034 to April 2035.

Table 7 presents the SWSI change percentages between 2023 and 2042 in comparison to the preceding period for the MIROC-ES2L model across the three mentioned scenarios. It is evident that during the months of January and February, across all three scenarios and time scales of 1 and 3 months, the SWSI value were increased, indicating a decrease in basin dryness. The highest increase is observed during January under scenario SSP1-2.6, with a reduction in basin drought levels nearly 60 times greater compared to previous conditions. Additionally, in the months of October, November, and December, across time scales of 1, 3, and 6 months, drought levels decrease consistently under all scenarios. Across all scenarios and within the 12-month time scale, the wet season months (February, March, April, and May) experience an increase in dryness, indicating a drier basin. The most significant increase in dryness within this time frame is observed in February, particularly under scenario SSP5-8.5, where it reaches a substantial −86.84%.

Discussion

Various studies investigating the impact of climate change on the environment have produced reasonable results using models from CMIP3 to CMIP6 (Sherafati and Pezeshki 2020, Shadkam et al. 2016, Vaghefi et al. 2019, Samavati et al. 2023, and Peres et al. 2023). In this study, CMIP6 models and scenarios were employed to assess the effects of climate change on runoff and hydrological drought. Among the models considered, the MIROC-ES2L model demonstrated

Table 6 Percent of changes in runoff monthly variations for all used models and scenarios compared to the past

	ACCESS-CM2 (%)	CNRM-CM6-1 (%)	CNRM-ESM2-1 (%)	INM-CM4-8 (%)	INM-CM5-0 (%)	MIROC6 (%)	MIROC-ES2L (%)	Average (%)
SSP1-2.6								
January	−37.49	93.93	−39.36	−37.28	14.74	−21.35	−73.60	−14.34
February	−63.58	134.22	−50.73	−40.80	37.71	15.77	−79.88	−6.76
March	20.00	44.94	12.60	58.39	22.62	42.88	6.78	29.74
April	6.60	−33.12	6.04	20.93	−39.37	−24.68	11.90	−7.39
May	7.82	−53.10	−14.99	−22.12	−63.91	−50.76	−7.61	−29.24
June	−1.31	−61.85	−30.28	−37.07	−66.95	−60.64	−24.31	−40.34
July	−17.74	−67.65	−40.74	−46.60	−71.76	−65.34	−38.09	−49.70
August	123.13	−4.91	124.81	48.00	−15.87	0.88	65.61	48.81
September	1283.95	592.87	1383.33	861.09	455.85	555.78	908.14	863.00
October	107.80	129.50	90.09	−3.43	50.46	88.98	98.99	80.34
November	86.59	221.62	68.34	−47.79	37.85	63.15	4.72	62.07
December	80.55	262.77	100.06	−10.22	113.18	75.13	−7.81	87.67
SSP2-4.5								
January	−43.83	144.99	−43.11	−41.33	12.85	0.30	−55.79	−3.70
February	−74.86	167.59	−45.52	−45.28	24.13	12.10	−68.72	−4.36
March	35.38	78.97	−0.18	40.03	20.47	20.17	39.15	33.43
April	28.73	−27.82	5.09	9.09	−42.59	−33.37	27.58	−4.75
May	6.35	−56.94	−8.99	−24.33	−62.23	−48.41	17.49	−25.29
June	−10.12	−64.75	−25.89	−37.76	−63.41	−57.24	−4.47	−37.67
July	−21.83	−55.89	−18.61	−46.94	−68.96	−63.62	−21.93	−42.54
August	122.91	38.54	151.10	47.10	−6.10	1.72	115.70	67.28
September	1348.37	1092.02	1438.72	848.37	571.20	567.95	1259.26	1017.98
October	198.65	256.91	106.86	88.56	94.11	68.84	172.49	140.92
November	164.38	180.60	82.47	−19.69	45.68	66.88	47.16	81.07
December	102.50	319.14	69.94	13.01	108.30	140.03	19.00	110.27
SSP5-8.5								
January	−30.08	129.03	−49.43	−43.00	−6.91	−19.31	−73.44	−13.31
February	−52.72	147.64	−51.02	−43.61	29.54	5.55	−79.50	−6.30
March	18.44	42.82	−4.12	65.87	17.31	6.13	9.81	22.32
April	31.43	−43.30	10.07	21.70	−45.92	−42.01	33.22	−4.97
May	2.88	−61.90	−10.81	−19.92	−63.84	−57.82	14.85	−28.08
June	−12.07	−66.88	−27.53	−36.95	−65.47	−64.71	−9.13	−40.39
July	−24.41	−71.25	−40.54	−45.72	−71.85	−69.77	−25.47	−49.77
August	113.29	−14.96	62.30	49.87	−17.10	−16.78	104.88	40.22
September	1279.11	527.83	963.84	860.81	488.41	438.14	1188.72	820.98
October	190.41	137.48	51.55	55.03	63.11	81.95	132.65	101.74
November	153.50	200.12	41.74	−21.35	7.70	43.89	−10.18	59.35
December	127.11	270.72	63.55	3.91	56.77	106.40	5.74	90.60

the most accurate prediction for the Ekbatan watershed, which is a mountainous watershed. The findings from a comparison between CMIP6 and CMIP5 models indicate that the ACCESS-CM2 and MIROC-ES2L models within CMIP6, along with the MIROC5 model in CMIP5, exhibit strong predictive capabilities for precipitation, as reported by Kamruzzaman et al. (2021). Additionally, Zamani et al. (2020) have reported that CMIP5 outperforms CMIP6

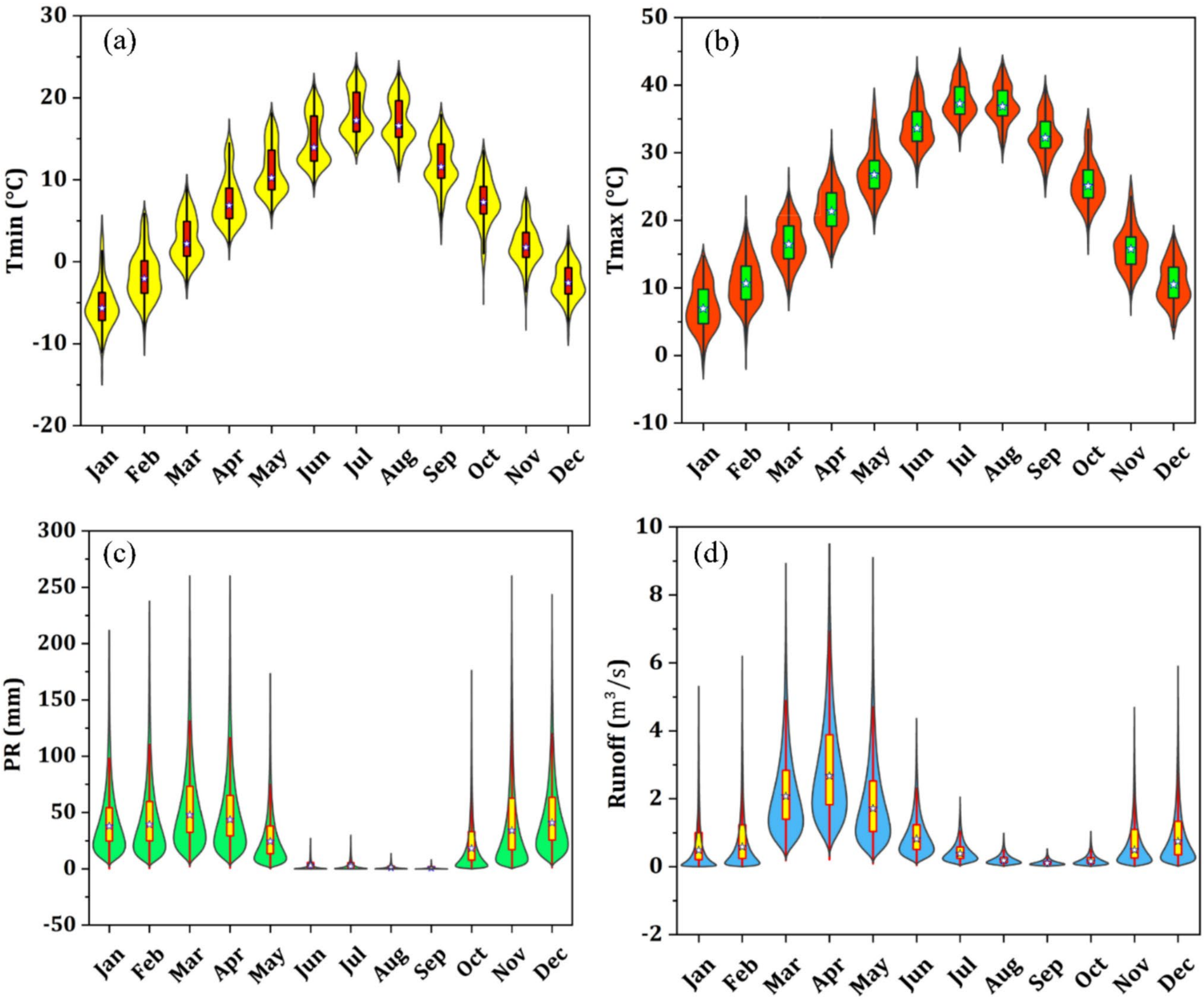

Fig. 8 Violin plots to evaluate the monthly pattern of air temperature, precipitation and runoff distributions in the Ekbatan watershed

during the autumn season; however, it's worth noting that overall, CMIP6 exhibits lower accuracy in predicting both precipitation and temperature. Recent studies in Iran have highlighted the superior performance of several selected models in this study for projecting key climate parameters. For instance, Niroumandfard et al. (2022) and Shoja and Shamsipour (2023) evaluated CMIP6 models for temperature and precipitation projections and identified CNRM and MIROC variants as top-performing models due to their accuracy in capturing regional climate patterns and variability under SSP scenarios. Moreover, studies in regions with climates comparable to that of the Ekbatan watershed further support our model selection. Abdolalizadeh et al. (2023) and Ershadfath et al. (2022) assessed CMIP6 models in areas with hydrological and topographic similarities to our study region, collectively identifying models such as INM-CM5-0, ACCESS, and MIROC-ES2L as particularly effective in reproducing observed trends and projecting future climate conditions. The runoff simulation in the study area was conducted using the semi-distributed SWAT model, which generally performed well. However, there was a relative error in simulating the peak runoff, which aligns with the findings of Sharafati and Pezeshki (2020) and Zakizadeh et al. (2021). Nevertheless, this limitation does not impede the investigation of hydrological drought, which remains the primary focus of our study. The outcomes from simulating future runoff patterns in response to climate change indicate that during the dry months (June, July, August, and

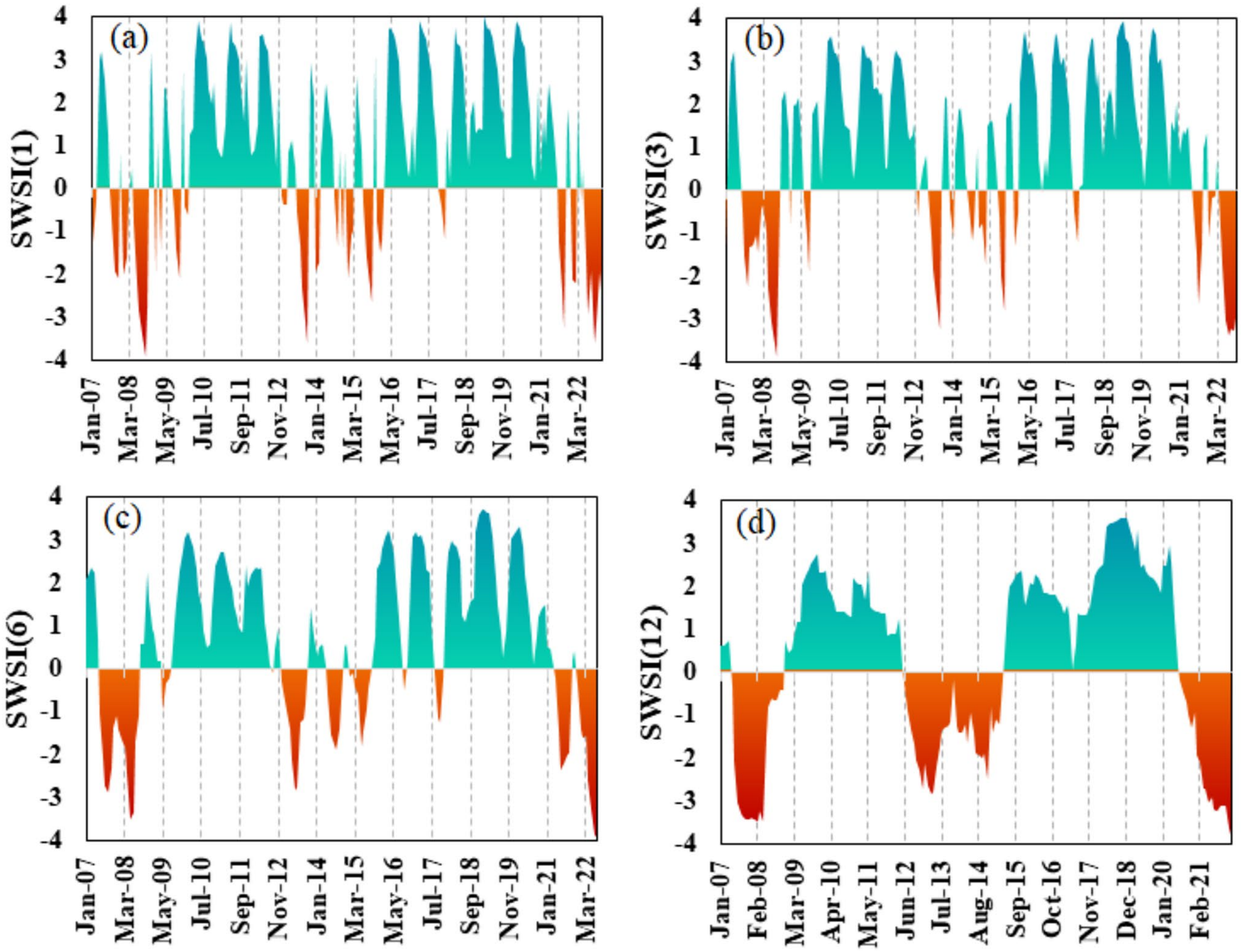

Fig. 9 Monthly variations in SWSI in Ekbatan watershed (2007–2022) in different timescales: **a** 1 month, **b** 3 month, **c** 6 month and **d** 12 month

September), despite the absence of precipitation, runoff will still occur due to the mountainous area and presence of snow cover in the watershed. In this study, the hydrological drought in the basin was examined using the SWSI index. Unlike other hydrological drought indicators that solely consider runoff, the SWSI index incorporates parameters of precipitation, runoff, and water storage volume in the basin. This comprehensive approach enable researcher for better prediction of drought. This finding is supported by the works of Aghelpour (2021) and Tareke and Awoke (2022), reflecting the significance of considering multiple factors in assessing drought conditions in a catchment. The SWSI index was utilized in this study to examine the impact of climate change on hydrological drought in the basin. Results from three future scenarios indicate that traditionally in dry months runoff, will be increased in the study region. It seems that this trend is partly due to the mountainous terrain of the basin and the anticipated rise in air temperatures between 2023 and 2042. As air temperature increases during the warm months, snowmelt will accelerate, leading to heightened runoff. These findings are consistent with the results of Zakizadeh et al (2021) who studied similar work in the Darabad basin of Tehran, Iran, which used the CanESM2 model under RCP2.6, RCP4.5, and RCP8.5 scenarios. In contrast, Abbaszadeh et al. (2023) predicts a decrease in runoff in the arid region of southern Iran due to higher temperatures and increased evaporation. Several studies have examined the impact of climate change on future droughts in different regions. For instance, Lotfirad et al. (2021) conducted a study in southwest Iran, Jehanzaib et al. (2020) in northern South Korea, Peres et al. (2023) in Italy, and Gond et al. (2023) in northern India. The findings of these

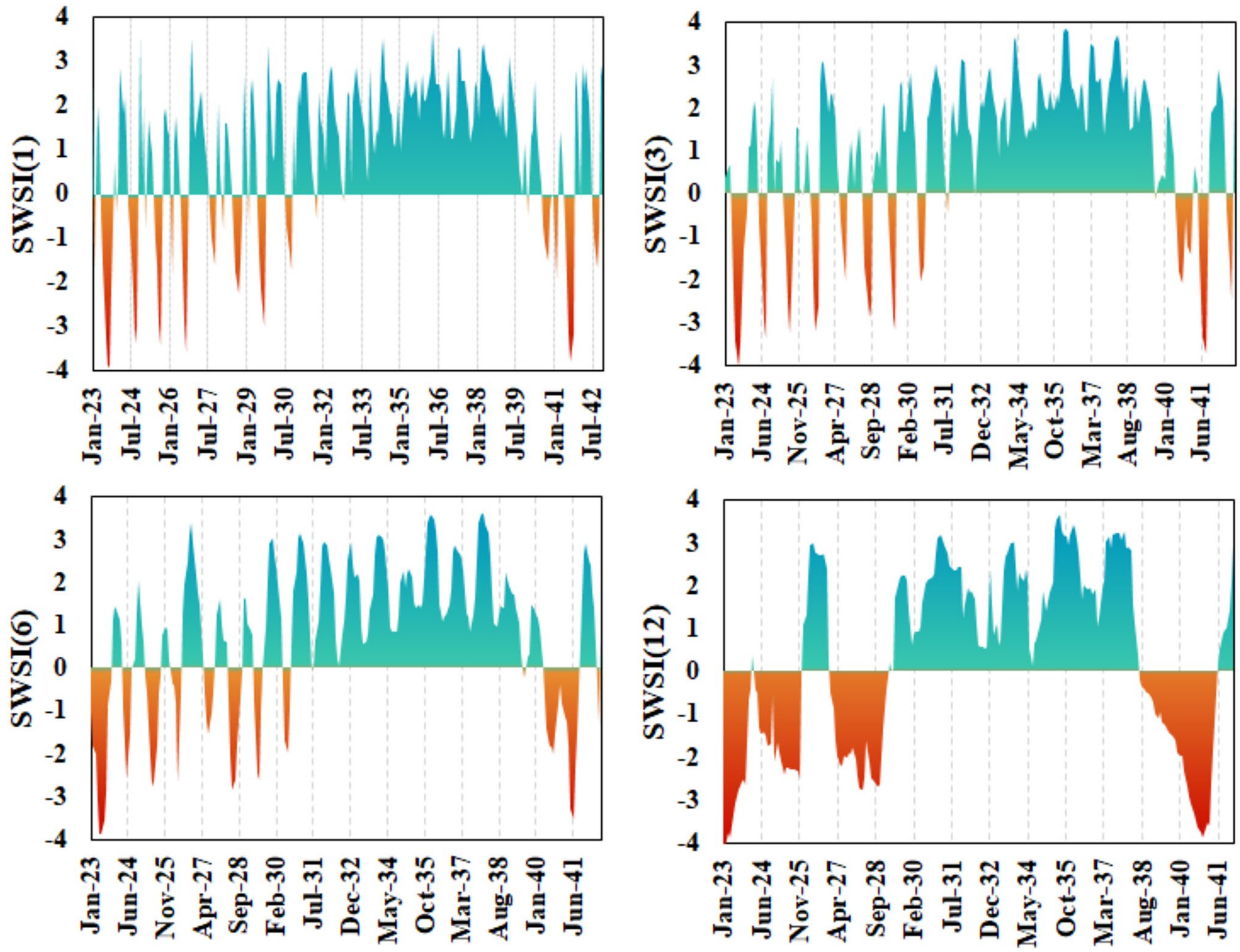

Fig. 10 Monthly variations in SWSI in the future period at 1, 3, 6, and 12- month timescales in Ekbatan watershed under MIROC-ES2L model and the SSP1-2.6 scenario (2023–2042)

studies indicate that meteorological droughts are expected to increase due to rising air temperatures and increased evapotranspiration. However, in a recent study, it was observed that dryness increased during the wet months of the year (February, March, April, and May), but decreased during the dry months of the year (August, September, and October). This could be attributed to the mountainous topography of the basin and its snowy regime.

Conclusion

The study utilized various models and scenarios from the CMIP6 dataset, including ACCESS-CM2, CNRM-CM6-1, CNRM-ESM2-1, INM-CM4-8, INM-CM5-0, MIROC6, and MIROC-ES2L. The findings showed that out of all the used models, MIROC-ES2L was the most accurate model with the least amount of error when studying the impact of climate change on hydrological drought in the mountainous basin. Also, the runoff simulation outcomes using the SWAT model in the watershed demonstrate a satisfactory level of accuracy for the model. The projections for future runoff, influenced by the climate models mentioned above, indicated that the ACCESS-CM2 model predicts the highest runoff, while the MIROC6 model anticipates the lowest runoff levels. The analysis of future runoff changes from 2023 to 2042 compared to the previous period (2000 to 2020) reveals that there will be an increase in runoff during the dry months of the year, with September experiencing the highest increase of 1017% under the SSP2-4.5 scenario. Considering

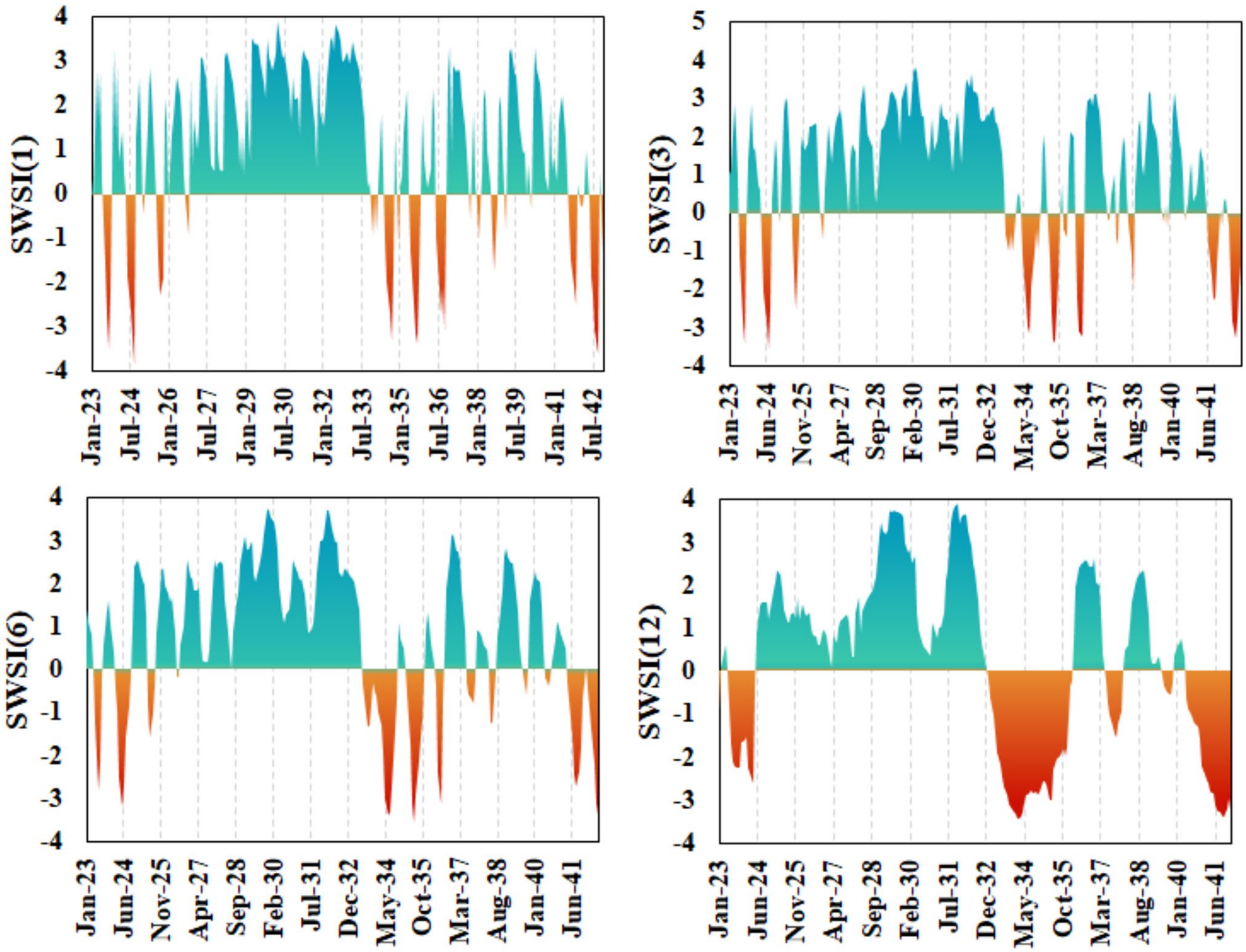

Fig. 11 Monthly variations in SWSI in the future period at 1, 3, 6, and 12- month timescales in Ekbatan watershed under MIROC-ES2L model and the SSP2-4.5 scenario (2023–2042)

a nearly ten-fold increase in runoff during warm months, it can be inferred that the intensity of instantaneous runoff in mountainous basins is on the rise. Conversely, there will be a decrease in runoff during the wet months of the year. The analysis of the runoff trend during the period from 2023 to 2042 indicates that, for the most part, there will be no significant increase or decrease in runoff across mentioned models and scenarios. However, the CNRM-CM6-1 model under the SSP5-8.5 scenario showed increasing trend in runoff at the 95% confidence level. The SWSI analysis outcomes for the top-performing model, MIROC-ES2L, indicate that, under the SSP1-2.6 scenario, the basin is projected to undergo a sustained wet phase spanning from 2024 to 2033. In contrast, under the SSP5-8.5 scenario, this prolonged wet period is expected to shift to the years 2037 to 2042. Overall, across all scenarios, the findings indicated a reduction in drought severity during the dry months of the year (August, September, and October), while conversely, an increase in drought severity is projected for the wet months of the year (February, March, April and May). The study's evidence demonstrates that climate change will exacerbate drought during the wet months of the year and intensify runoff volume

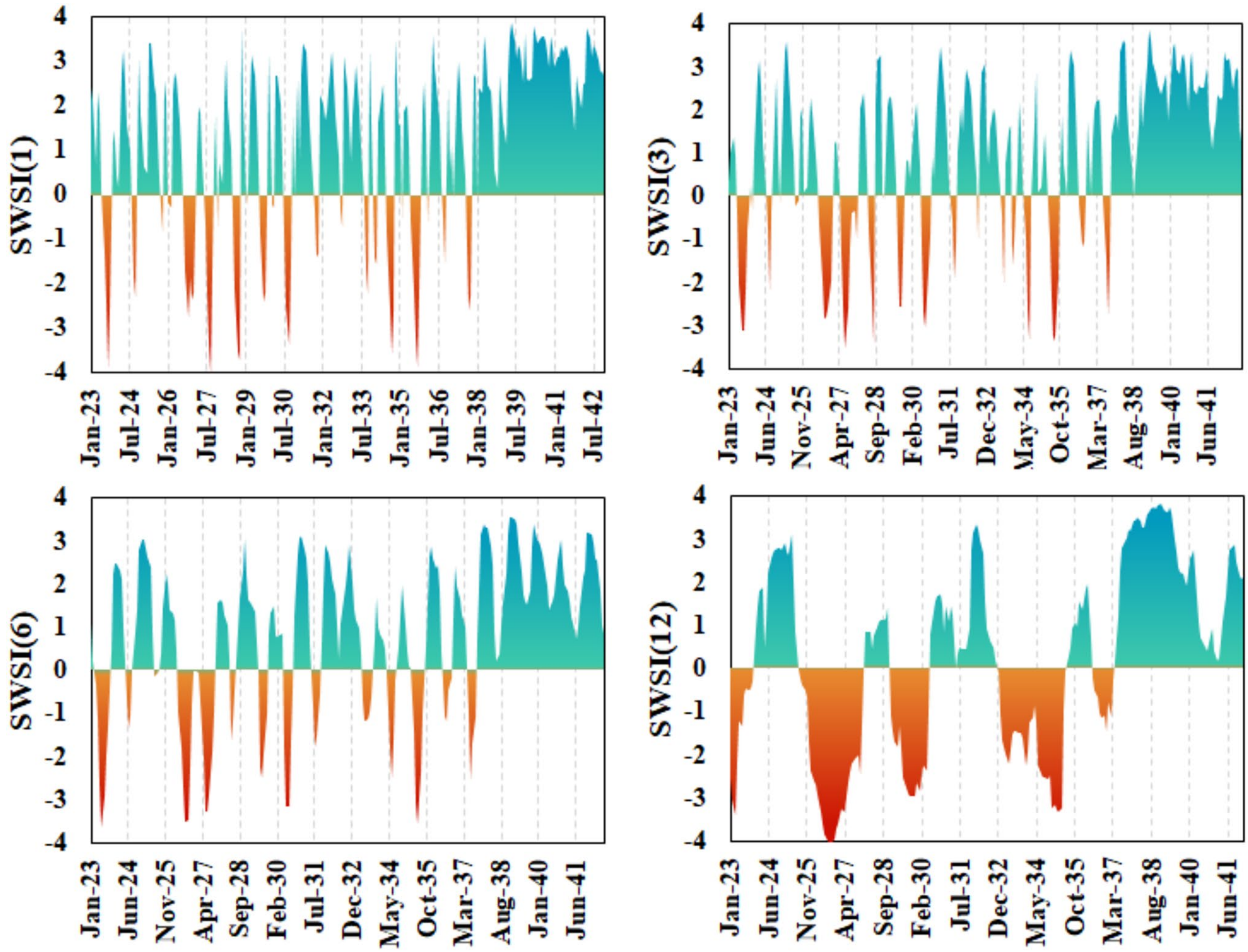

Fig. 12 Monthly variations in SWSI in the future period at 1, 3, 6, and 12- month timescales in Ekbatan watershed under MIROC-ES2L model and the SSP5-8.5 scenario (2023–2042)

Table 7 Percentage changes in future SWSI variations compared to the base period on MIROC-ES2L model in Ekbatan basin

	SSP1-2.6 (%)				SSP2-4.5 (%)				SSP5-8.5 (%)			
	1	3	6	12	1	3	6	12	1	3	6	12
January	291.23	6053.92	22.23	34.78	260.08	5571.84	16.67	−19.19	257.37	4391.70	34.12	−22.61
February	3266.48	19.55	3.11	−55.12	3279.04	16.46	1.57	−15.19	3611.39	26.86	18.38	−86.84
March	131.54	0.65	−3.57	−45.34	116.35	1.07	−5.21	−8.46	163.23	8.81	11.85	−73.32
April	1.11	−14.66	−42.82	−51.56	3.41	−12.33	−28.95	−22.79	20.20	−0.95	−7.84	−79.92
May	−23.63	−40.26	−229.75	−41.27	−13.35	−26.13	−151.88	−18.79	0.41	−15.31	−191.18	−55.04
June	−47.61	−90.00	−390.65	−18.95	−30.99	−61.02	−338.98	−21.70	−7.97	−55.48	−561.72	−37.45
July	−74.17	−196.92	−62.64	−0.63	−46.09	−145.46	−37.67	−16.08	−32.82	−198.21	−197.10	−15.02
August	−142.57	−166.34	91.16	24.87	−89.30	−137.52	81.32	−2.66	−107.93	−272.06	−22.08	−1.09
September	−366.35	−65.10	367.87	40.14	−180.98	−55.34	265.08	−11.71	−463.96	−179.68	228.92	5.93
October	44.94	28.41	282.31	48.74	72.64	1.68	210.02	−17.24	−58.64	4.27	297.18	11.18
November	42.84	54.22	48.82	71.24	47.68	38.73	31.61	−13.25	69.39	50.75	63.21	0.66
December	148.80	1073.75	41.05	75.25	51.57	646.97	19.73	−23.95	142.17	468.54	42.63	−17.51

during the dry months of the year, which is one of the main results of this research in mountainous basins. Therefore, it is crucial to prioritize efforts to mitigate these effects.

Acknowledgements The authors are grateful to the National Elite Foundation of Iran and the University of Tabriz for providing the post-doctoral fellowship that made this research possible.

Authors contribution OB Conceptualization, visualization, methodology, software, coding, and writing original draft; YD Supervision, reviewing, editing, and validation; AS Methodology; FS Methodology.

Funding No direct funding was received for this research.

Data availability The corresponding author can provide access to any data, models, or codes that were utilized in this study upon receiving a reasonable request.

Declarations

Conflicts of interest The authors declare no conflict of interest.

Consent to participate The authors volunteered to take part in this research project.

Consent for publication This study's publishing was approved by the authors.

Compliance with ethical standards The authors have mutually agreed to submit this paper exclusively to this journal and it is not being considered for review by any other publications at this time.

References

Abbaspour KC, Rouholahnejad E, Vaghefi S, Srinivasan R, Yang H, Kløve B (2015) A continental-scale hydrology and water quality model for Europe: calibration and uncertainty of a high-resolution large-scale SWAT model. J Hydrol 524:733–752. https://doi.org/10.1016/j.jhydrol.2015.03.027

Abbaszadeh M, Bazrafshan O, Mahdavi R, Sardooi ER, Jamshidi S (2023) Modeling future hydrological characteristics based on land use/land cover and climate changes using the SWAT model. Water Resour Manag 37:4177–4194. https://doi.org/10.1007/s11269-023-03545-6

Abbaspour KC, Yang J, Maximov I, Siber R, Bogner K, Mieleitner J, Srinivasan R (2007) Modelling hydrology and water quality in the pre-alpine/alpine Thur watershed using SWAT. J Hydrol 333(2–4):413–430. https://doi.org/10.1016/j.jhydrol.2006.09.014

Abdolalizadeh F, Mohammad Khorshiddoust A, Jahanbakhsh S (2023) Projection of the future outlook of temperature and precipitation in Urmia Lake basin by the CMIP6 models. Phys Geogr Res 55(1):95–112. https://doi.org/10.22059/jphgr.2023.352727.1007737

Abdulai PJ, Chung ES (2019) Uncertainty assessment in drought severities for the Cheongmicheon watershed using multiple GCMs and the reliability ensemble averaging method. Sustainability 11(16):4283. https://doi.org/10.3390/su11164283

Aghelpour P, Bahrami-Pichaghchi H, Varshavian V (2021) Hydrological drought forecasting using multi-scalar streamflow drought index, stochastic models and machine learning approaches, in northern Iran. Stoch Environ Res Risk Assess 35:1615–1635. https://doi.org/10.1007/s00477-020-01949-z

Ahmadi M, Moeini A, Ahmadi H, Motamedvaziri B, Zehtabiyan GR (2019) Comparison of the performance of SWAT, IHACRES and artificial neural networks models in rainfall-runoff simulation (case study: Kan watershed, Iran). Phys Chem Earth Parts a/b/c 111:65–77. https://doi.org/10.1016/j.pce.2019.05.002

Aliyari F, Bailey RT, Tasdighi A, Dozier A, Arabi M, Zeiler K (2019) Coupled SWAT-MODFLOW model for large-scale mixed agro-urban river basins. Environ Model Softw 115:200–210. https://doi.org/10.1016/j.envsoft.2019.02.014

Andrade CW, Montenegro SM, Montenegro AA, Lima JRDS, Srinivasan R, Jones CA (2021) Climate change impact assessment on water resources under RCP scenarios: a case study in Mundaú River Basin, Northeastern Brazil. Int J Climatol 41:E1045–E1061. https://doi.org/10.1002/joc.6751

Andrade MA, Mello CRD, Beskow S (2013) Simulação hidrológica em uma bacia hidrográfica representativa dos Latossolos na região Alto Rio Grande, MG. Revista Brasileira De Engenharia Agrícola e Ambiental 17:69–76. https://doi.org/10.1590/S1415-43662013000100010

Arnold J (1994) SWAT-soil and water assessment tool

Arnold JG, Srinivasan R, Muttiah RS, Williams JR (1998) Large area hydrologic modeling and assessment part I: model development. JAWRA J Am Water Resour Assoc 34(1):73–89. https://doi.org/10.1111/j.1752-1688.1998.tb05961.x

Babaeian F, Delavar M, Morid S, Srinivasan R (2021) Robust climate change adaptation pathways in agricultural water management. Agric Water Manag 252:106904. https://doi.org/10.1016/j.agwat.2021.106904

Babamiri O, Dinpashoh Y (2024) Uncertainty analysis of river water quality based on stochastic optimization of waste load allocation using the generalized likelihood uncertainty estimation method. Water Resour Manag 38(3):967–989. https://doi.org/10.1007/s11269-023-03704-9

Babamiri O, Azari A, Marofi S (2022) An integrated fuzzy optimization and simulation method for optimal quality-quantity operation of a reservoir-river system. Water Supply 22(4):4207–4229. https://doi.org/10.2166/ws.2022.045

Babaousmail H, Ayugi B, Rajasekar A, Zhu H, Oduro C, Mumo R, Ongoma V (2022) Projection of extreme temperature events over the Mediterranean and Sahara using bias-corrected CMIP6 models. Atmosphere 13(5):741. https://doi.org/10.3390/atmos13050741

Bhatta B, Shrestha S, Shrestha PK, Talchabhadel R (2019) Evaluation and application of a SWAT model to assess the climate change impact on the hydrology of the Himalayan River Basin. CATENA 181:104082. https://doi.org/10.1016/j.catena.2019.104082

Blainski É, Acosta E, Nogueira PCDP (2017) Calibração e validação do modelo SWAT para simulação hidrológica em uma bacia hidrográfica do litoral norte catarinense. Revista Ambiente & Água 12:226–237. https://doi.org/10.4136/ambi-agua.1951

Chang HS, Su Q (2021) Exploring the coupling relationship of stormwater runoff distribution in watershed from the perspective of fairness. Urban Clim 36:100792. https://doi.org/10.1016/j.uclim.2021.100792

Chen Y, Xu CY, Chen X, Xu Y, Yin Y, Gao L, Liu M (2019) Uncertainty in simulation of land-use change impacts on catchment runoff with multi-timescales based on the comparison of the HSPF and SWAT models. J Hydrol 573:486–500. https://doi.org/10.1016/j.jhydrol.2019.03.091

Cibin R, Sudheer KP, Chaubey I (2010) Sensitivity and identifiability of stream flow generation parameters of the SWAT model. Hydrol Process Int J 24(9):1133–1148. https://doi.org/10.1002/hyp.7568

de Andrade CW, Montenegro SM, Montenegro AA, Lima JRDS, Srinivasan R, Jones CA (2019) Soil moisture and discharge modeling in a representative watershed in northeastern Brazil using SWAT. Ecohydrol Hydrobiol 19(2):238–251. https://doi.org/10.1016/j.ecohyd.2018.09.002

dos Santos JYG, Montenegro SMGL, da Silva RM, Santos CAG, Quinn NW, Dantas APX, Neto AR (2021) Modeling the impacts of future LULC and climate change on runoff and sediment yield in a strategic basin in the Caatinga/Atlantic forest ecotone of Brazil. CATENA 203:105308. https://doi.org/10.1016/j.catena.2021.105308

Ershadfath F, Raeini Sarjaz M, Shahnazari A, Eivind Olesen J (2022) Application of linear scaling post-processing method for bias correction of climate models retrieved from CMIP6. Iran-Water Resour Res 18(3):131–144

Escanilla-Minchel R, Alcayaga H, Soto-Alvarez M, Kinnard C, Urrutia R (2020) Evaluation of the impact of climate change on runoff generation in an andean glacier watershed. Water 12(12):3547. https://doi.org/10.3390/w12123547

Fereidoon M, Koch M, Brocca L (2019) Predicting rainfall and runoff through satellite soil moisture data and SWAT modelling for a poorly gauged basin in Iran. Water 11(3):594. https://doi.org/10.3390/w11030594

Gebremariam SY, Martin JF, DeMarchi C, Bosch NS, Confesor R, Ludsin SA (2014) A comprehensive approach to evaluating watershed models for predicting river flow regimes critical to downstream ecosystem services. Environ Model Softw 61:121–134. https://doi.org/10.1016/j.envsoft.2014.07.004

Gond S, Gupta N, Dikshit PKS, Patel J (2023) Assessment of drought variability using SPEI under observed and projected climate scenarios over Uttar Pradesh, India. Phys Chem Earth 131:103440. https://doi.org/10.1016/j.pce.2023.103440

Goyal MK, Panchariya VK, Sharma A, Singh V (2018) Comparative assessment of SWAT model performance in two distinct catchments under various DEM scenarios of varying resolution, sources and resampling methods. Water Resour Manag 32:805–825. https://doi.org/10.1007/s11269-017-1840-1

Gupta V, Singh V, Jain MK (2020) Assessment of precipitation extremes in India during the 21st century under SSP1-1.9 mitigation scenarios of CMIP6 GCMs. Journal of Hydrology 590:125422. https://doi.org/10.1016/j.jhydrol.2020.125422

Hammouri N, Adamowski J, Freiwan M, Prasher S (2017) Climate change impacts on surface water resources in arid and semi-arid regions: a case study in northern Jordan. Acta Geod Geoph 52:141–156. https://doi.org/10.1007/s40328-016-0163-7

Hargreaves GH, Samani ZA (1985) Reference crop evapotranspiration from temperature. Appl Eng Agri 1(2):96–99. https://doi.org/10.13031/2013.26773

Hobart M, Schirrmann M, Abubakari AH, Badu-Marfo G, Kraatz S, Zare M (2024) Drought monitoring and prediction in agriculture: employing earth observation data, climate scenarios and data driven methods; a case study: mango orchard in tamale. Ghana Remote Sens 16(11):1942. https://doi.org/10.3390/rs16111942

Hyung-Joong K (2006) Evaluation of semi-distributed hydrological drought using SWSI (Surface Water Supply Index). J Korean Soc Agric Eng 48(2):37–43

Jehanzaib M, Shah SA, Yoo J, Kim TW (2020) Investigating the impacts of climate change and human activities on hydrological drought using non-stationary approaches. J Hydrol 588:125052. https://doi.org/10.1016/j.jhydrol.2020.125052

Kaffas K, Hrissanthou V, Sevastas S (2018) Modeling hydromorphological processes in a mountainous basin using a composite mathematical model and ArcSWAT. CATENA 162:108–129. https://doi.org/10.1016/j.catena.2017.11.017

Kamali B, Houshmand Kouchi D, Yang H, Abbaspour KC (2017) Multilevel drought hazard assessment under climate change scenarios in semi-arid regions—a case study of the Karkheh river basin in Iran. Water 9(4):241. https://doi.org/10.3390/w9040241

Kamruzzaman M, Shahid S, Islam AT, Hwang S, Cho J, Zaman MAU, Hossain MB (2021) Comparison of CMIP6 and CMIP5 model performance in simulating historical precipitation and temperature in Bangladesh: a preliminary study. Theor Appl Climatol 145:1385–1406. https://doi.org/10.1007/s00704-021-03691-0

Kendall MG (1975) Rank correlation methods. Charles Griffin, London

Khazaei M, Mirzaei MR (2013) Comparison of monthly discharge prediction efficiency using artificial neural network methods and time series. Watershed Eng Manag 5(2):74–84. https://doi.org/10.22092/ijwmse.2013.101803

Kiprotich P, Wei X, Zhang Z, Ngigi T, Qiu F, Wang L (2021) Assessing the impact of land use and climate change on surface runoff response using gridded observations and swat+. Hydrology 8(1):48. https://doi.org/10.3390/hydrology8010048

Kottek M, Grieser J, Beck C, Rudolf B, Rubel F (2006) World Map of the Köppen-Geiger climate classification updated. Meteorol Z 15:259–263. https://doi.org/10.1127/0941-2948/2006/0130

Li S, Xiong L, Dong L, Zhang J (2013) Effects of the Three Gorges Reservoir on the hydrological droughts at the downstream Yichang station during 2003–2011. Hydrol Process 27(26):3981–3993. https://doi.org/10.1002/hyp.9541

Li Z, Li Q, Wang J, Feng Y, Shao Q (2021) Corrigendum to "Impacts of projected climate change on runoff in upper reach of Heihe River basin using climate elasticity method and GCMs"[Sci Total Environ 716(2020) 137072]. Sci Tot Environ 766: 142628. https://doi.org/10.1016/j.scitotenv.2020.142628

Lian Y, Sun M, Wang J, Luan Q, Jiao M, Zhao X, Gao X (2021) Quantitative impacts of climate change and human activities on the runoff evolution process in the Yanhe River Basin. Phys Chem Earth Parts a/b/c 122:102998. https://doi.org/10.1016/j.pce.2021.102998

Liu Z, Herman JD, Huang G, Kadir T, Dahlke HE (2021) Identifying climate change impacts on surface water supply in the southern Central Valley, California. Sci Tot Environ 759:143429. https://doi.org/10.1016/j.scitotenv.2020.143429

Lotfirad M, Adib A, Salehpoor J, Ashrafzadeh A, Kisi O (2021) Simulation of the impact of climate change on runoff and drought in an arid and semiarid basin (the Hablehroud, Iran). Appl Water Sci 11:1–24. https://doi.org/10.1007/s13201-021-01494-2

Loucks DP, Stedinger JR, Haith DA (1981) Water Resource Systems Planning and Analysis. Prentice Hall, Englewood Cliffs

Luo M, Liu T, Meng F, Duan Y, Frankl A, Bao A, De Maeyer P (2018) Comparing bias correction methods used in downscaling precipitation and temperature from regional climate models: a case study from the Kaidu River Basin in Western China. Water 10(8):1046. https://doi.org/10.3390/w10081046

Mann HB (1945) Nonparametric tests against trend. Econometrica J Econom Soc, pp 245–259. https://doi.org/10.2307/1907187

Mishra AK, Singh VP (2010) A review of drought concepts. J Hydrol 391(1–2):202–216. https://doi.org/10.1016/j.jhydrol.2010.07.012

Moriasi DN, Arnold JG, Van Liew MW, Bingner RL, Harmel RD, Veith TL (2007) Model evaluation guidelines for systematic quantification of accuracy in watershed simulations. Trans ASABE 50(3):885–900

Muronda MT, Marofi S, Nozari H, Babamiri O (2021) Uncertainty analysis of reservoir operation based on stochastic optimization approach using the generalized likelihood uncertainty estimation method. Water Resour Manag 35(10):3179–3201. https://doi.org/10.1007/s11269-021-02877-5

Neitsch SL, Arnold JG, Kiniry JR, Williams JR (2011) Soil and water assessment tool theoretical documentation version 2009. Texas Water Resources Institute, College Station

Niroumandfard F, Khashei A, Hashemi R, Ghorbani K (2022) Investigation of climate change projection on temperature and precipitation parameters using CMIP6 Models (Case Study: Birjand Station). Iran J Soil Water Res 53(9):2009–2026. https://doi.org/10.22059/ijswr.2022.343936.669284

Peng L, Li Z (2021) Ensemble flood risk assessment in the Yangtze River economic belt under CMIP6 SSP-RCP scenarios. Sustainability 13(21):12097. https://doi.org/10.3390/su132112097

Pereira DDR, Martinez MA, Almeida AQD, Pruski FF, Silva DDD, Zonta JH (2014) Hydrological simulation using SWAT model in headwater basin in Southeast Brazil. Engenharia Agrícola 34:789–799. https://doi.org/10.1590/S0100-69162014000400018

Peres DJ, Bonaccorso B, Palazzolo N, Cancelliere A, Mendicino G, Senatore A (2023) A dynamic approach for assessing climate change impacts on drought: an analysis in Southern Italy. Hydrol Sci J 68(9):1213–1228. https://doi.org/10.1080/02626667.2023.2217332

Rajib MA, Merwade V, Yu Z (2016) Multi-objective calibration of a hydrologic model using spatially distributed remotely sensed/in-situ soil moisture. J Hydrol 536:192–207. https://doi.org/10.1016/j.jhydrol.2016.02.037

Ridwansyah I, Yulianti M, Apip Onodera SI, Shimizu Y, Wibowo H, Fakhrudin M (2020) The impact of land use and climate change on surface runoff and groundwater in Cimanuk watershed, Indonesia. Limnology 21:487–498. https://doi.org/10.1007/s10201-020-00629-9

Salimi H, Asadi E, Darbandi S (2021) Meteorological and hydrological drought monitoring using several drought indices. Appl Water Sci 11:1–10. https://doi.org/10.1007/s13201-020-01345-6

Samavati A, Babamiri O, Rezai Y, Heidarimozaffar M (2023) Investigating the effects of climate change on future hydrological drought in mountainous basins using SWAT model based on CMIP5 model. Stoch Env Res Risk Assess 37(3):849–875. https://doi.org/10.1007/s00477-022-02319-7

Satoh Y, Yoshimura K, Pokhrel Y, Kim H, Shiogama H, Yokohata T, Oki T (2022) The timing of unprecedented hydrological drought under climate change. Nature communications 13(1):3287. https://doi.org/10.1038/s41467-022-30729-2

Shadkam S, Ludwig F, van Oel P, Kirmit Ç, Kabat P (2016) Impacts of climate change and water resources development on the declining inflow into Iran's Urmia Lake. J Great Lakes Res 42(5):942–952. https://doi.org/10.1016/j.jglr.2016.07.033

Shafer BA, Dezman LE (1982) Development of surface water supply index (SWSI) to assess the severity of drought condition in snowpack runoff areas. Proceeding of the Western Snow Conference, April, Reno, Nevada

Shaigan M, Alimohammadi A, Rouhani H (2011) Hydrological modeling of Taleghan basin in GIS environment using SWAT model. Iran Remote Sens GIS 3(2):1–18

Sharafati A, Pezeshki E (2020) A strategy to assess the uncertainty of a climate change impact on extreme hydrological events in the semi-arid Dehbar catchment in Iran. Theoret Appl Climatol 139:389–402. https://doi.org/10.1007/s00704-019-02979-6

Shoja F, Shamsipour A (2023) Projection of future precipitation changes in Tehran's water supply watersheds. J Nat Environ Hazards 12(36):151–180. https://doi.org/10.22111/jneh.2022.42622.1908

Siabi EK, Awafo EA, Kabo-bah AT, Derkyi NSA, Akpoti K, Mortey EM, Yazdanie M (2023) Assessment of shared socioeconomic pathway (SSP) climate scenarios and its impacts on the Greater Accra region. Urban Clim 49:101432. https://doi.org/10.1016/j.uclim.2023.101432

Su X, Li X, Niu Z, Liang X (2021) A new complexity-based three-stage method to comprehensively quantify positive/negative contribution rates of climate change and human activities to changes in runoff in the upper Yellow River. J Clean Prod 287:125017. https://doi.org/10.1016/j.jclepro.2020.125017

Taie Semiromi M, Koch M (2019) Analysis of spatio-temporal variability of surface–groundwater interactions in the Gharehsoo river basin, Iran, using a coupled SWAT-MODFLOW model. Environ Earth Sci 78:1–21. https://doi.org/10.1007/s12665-019-8206-3

Tan ML, Yusop Z, Chua VP, Chan NW (2017) Climate change impacts under CMIP5 RCP scenarios on water resources of the Kelantan River Basin, Malaysia. Atmos Res 189:1–10. https://doi.org/10.1016/j.atmosres.2017.01.008

Tareke KA, Awoke AG (2022) Hydrological drought analysis using streamflow drought index (SDI) in Ethiopia. Adv Meteorol 2022(1):7067951

Teutschbein C, Seibert J (2012) Bias correction of regional climate model simulations for hydrological climate-change impact studies: review and evaluation of different methods. J Hydrol 456:12–29. https://doi.org/10.1016/j.jhydrol.2012.05.052

Vaghefi SA, Keykhai M, Jahanbakhshi F, Sheikholeslami J, Ahmadi A, Yang H, Abbaspour KC (2019) The future of extreme climate in Iran. Sci Rep 9(1):1464. https://doi.org/10.1038/s41598-018-38071-8

Van Loon AF (2015) Hydrological drought explained. Wiley Interdiscip Rev Water 2(4):359–392. https://doi.org/10.1002/wat2.1085

Vasiliades L, Loukas A, Liberis N (2011) A water balance derived drought index for Pinios River Basin, Greece. Water Resour Manag 25:1087–1101. https://doi.org/10.1007/s11269-010-9665-1

Wang Z, Zhong R, Lai C, Zeng Z, Lian Y, Bai X (2018) Climate change enhances the severity and variability of drought in the Pearl River Basin in South China in the 21st century. Agric For Meteorol 249:149–162. https://doi.org/10.1016/j.agrformet.2017.12.077

Wodaje GG, Asfaw ZE, Denboba MA (2021) Impacts and uncertainties of climate change on stream flow of the Bilate River (Ethiopia), using a CMIP5 general circulation models ensemble. Int J Water Resour Environ Eng 13(1):64–75. https://doi.org/10.5897/IJWREE2020.0973

Xue C, Chen B, Wu H (2014) Parameter uncertainty analysis of surface flow and sediment yield in the Huolin Basin, China. J Hydrol Eng 19(6):1224–1236. https://doi.org/10.1061/(ASCE)HE.1943-5584.0000909

Xue D, Zhou J, Zhao X, Liu C, Wei W, Yang X, Zhao Y (2021) Impacts of climate change and human activities on runoff change in a typical arid watershed, NW China. Ecol Indic 121:107013. https://doi.org/10.1016/j.ecolind.2020.107013

Yao Y, Qu W, Lu J, Cheng H, Pang Z, Lei T, Tan Y (2021) Responses of hydrological processes under different shared socioeconomic pathway scenarios in the Huaihe River Basin, China. Water 13(8):1053. https://doi.org/10.3390/w13081053

Zakizadeh HR, Ahmadi H, Zehtabiyan GR, Moeini A, Moghaddamnia A (2021) Impact of climate change on surface runoff: a case study of the Darabad River, Northeast of Iran. J Water Clim Change 12(1):82–100. https://doi.org/10.2166/wcc.2020.089

Zamani Y, Hashemi Monfared SA, Azhdari Moghaddam M, Hamidianpour M (2020) A comparison of CMIP6 and CMIP5 projections for precipitation to observational data: the case of Northeastern Iran. Theoret Appl Climatol 142:1613–1623. https://doi.org/10.1007/s00704-020-03406-x

Zhang D, Chen X, Yao H, Lin B (2015) Improved calibration scheme of SWAT by separating wet and dry seasons. Ecol Model 301:54–61. https://doi.org/10.1016/j.ecolmodel.2015.01.018